Germline and Mosaic Variants in *PRKACA* and *PRKACB* Cause a Multiple Congenital Malformation Syndrome

Adrian Palencia-Campos,[1,2,27] Phillip C. Aoto,[3,27] Erik M.F. Machal,[4,27] Ana Rivera-Barahona,[1,2] Patricia Soto-Bielicka,[1] Daniela Bertinetti,[4] Blaine Baker,[3] Lily Vu,[3] Francesca Piceci-Sparascio,[5] Isabella Torrente,[5] Eveline Boudin,[6] Silke Peeters,[6] Wim Van Hul,[6] Celine Huber,[7,8] Dominique Bonneau,[9,10] Michael S. Hildebrand,[11,12] Matthew Coleman,[11,12] Melanie Bahlo,[13,14] Mark F. Bennett,[11,13,14] Amy L. Schneider,[11] Ingrid E. Scheffer,[11,12,15] Maria Kibæk,[16] Britta S. Kristiansen,[17] Mahmoud Y. Issa,[18] Mennat I. Mehrez,[19] Samira Ismail,[18] Jair Tenorio,[2,20,21] Gaoyang Li,[22] Bjørn Steen Skålhegg,[22] Ghada A. Otaify,[18] Samia Temtamy,[18] Mona Aglan,[18] Aia E. Jønch,[17] Alessandro De Luca,[5] Geert Mortier,[6,23] Valérie Cormier-Daire,[7,8] Alban Ziegler,[9,10] Mathew Wallis,[24,25] Pablo Lapunzina,[2,20,21] Friedrich W. Herberg,[4,28] Susan S. Taylor,[3,26,28] and Victor L. Ruiz-Perez[1,2,20,21,28,*]

Summary

PRKACA and *PRKACB* code for two catalytic subunits (Cα and Cβ) of cAMP-dependent protein kinase (PKA), a pleiotropic holoenzyme that regulates numerous fundamental biological processes such as metabolism, development, memory, and immune response. We report seven unrelated individuals presenting with a multiple congenital malformation syndrome in whom we identified heterozygous germline or mosaic missense variants in *PRKACA* or *PRKACB*. Three affected individuals were found with the same *PRKACA* variant, and the other four had different *PRKACB* mutations. In most cases, the mutations arose *de novo*, and two individuals had offspring with the same condition. Nearly all affected individuals and their affected offspring shared an atrioventricular septal defect or a common atrium along with postaxial polydactyly. Additional features included skeletal abnormalities and ectodermal defects of variable severity in five individuals, cognitive deficit in two individuals, and various unusual tumors in one individual. We investigated the structural and functional consequences of the variants identified in *PRKACA* and *PRKACB* through the use of several computational and experimental approaches, and we found that they lead to PKA holoenzymes which are more sensitive to activation by cAMP than are the wild-type proteins. Furthermore, expression of *PRKACA* or *PRKACB* variants detected in the affected individuals inhibited hedgehog signaling in NIH 3T3 fibroblasts, thereby providing an underlying mechanism for the developmental defects observed in these cases. Our findings highlight the importance of both Cα and Cβ subunits of PKA during human development.

Protein kinase A (PKA) can be found as an inactive tetrameric holoenzyme formed by the association of two catalytic (C) subunits with a regulatory (R) subunit dimer. Activation is achieved through binding of two molecules of cyclic AMP (cAMP) to each R-subunit and subsequent unleashing of the C-subunits to engage substrates. *PRKACA* (MIM: 601639) and *PRKACB* (MIM: 176892) code for the highly homologous Cα- and Cβ-subunits, respectively, and the four functionally non-redundant R-subunits (RIα, RIβ, RIIα, and RIIβ) are encoded by four genes (*PRKAR1A* [MIM: 188830], *PRKAR1B* [MIM: 176911], *PRKAR2A* [MIM: 176910], and *PRKAR2B* [MIM: 176912]).

[1]Instituto de Investigaciones Biomédicas "Alberto Sols," Consejo Superior de Investigaciones Científicas (CSIC)—Universidad Autónoma de Madrid (UAM), Madrid, 28029, Spain; [2]CIBER de Enfermedades Raras (CIBERER), Instituto de Salud Carlos III (ISCIII), Madrid, 28029, Spain; [3]Department of Pharmacology, University of California, San Diego, 9400 Gilman Drive, La Jolla, CA 92093-0654, USA; [4]Institute for Biology, Department of Biochemistry, University of Kassel, Kassel, 34132, Germany; [5]Medical Genetics Unit, Casa Sollievo della Sofferenza Foundation, IRCCS, San Giovanni Rotondo, 71013, Italy; [6]Department of Medical Genetics, University of Antwerp, Edegem, 2650, Belgium; [7]Clinical Genetics and Reference Center for Skeletal Dysplasia, AP-HP, Necker-Enfants Malades Hospital, Paris, 75015, France; [8]Université De Paris, INSERM UMR1163, Institut Imagine, Paris, 75015, France; [9]Biochemistry and Genetics Department, Angers Hospital, Angers Cedex 9, 49933, France; [10]UMR CNRS 6015—INSERM U1083, MitoVasc Institute, Angers University, Angers Cedex 9, 49933, France; [11]Epilepsy Research Centre, Department of Medicine, Austin Health, University of Melbourne, Heidelberg, 3084, Victoria, Australia; [12]Murdoch Children's Research Institute, Parkville, 3052, Victoria, Australia; [13]Population Health and Immunity Division, The Walter and Eliza Hall Institute of Medical Research, Parkville, 3052, Victoria, Australia; [14]Department of Medical Biology, University of Melbourne, Melbourne, 3010, Victoria, Australia; [15]Department of Paediatrics, University of Melbourne, Royal Children's Hospital, and Florey Institute of Neuroscience and Mental Health, Parkville, 3052, Victoria, Australia; [16]Children's Hospital of H.C. Andersen, Odense University Hospital, 5000 Odense, Denmark; [17]Department of Clinical Genetics, Odense University Hospital, 5000 Odense, Denmark; [18]Department of Clinical Genetics, Division of Human Genetics and Genome Research, Center of Excellence for Human Genetics, National Research Centre, Cairo, 12622, Egypt; [19]Department of Oro-dental Genetics, Division of Human Genetics and Genome Research. Center of Excellence for Human Genetics, National Research Centre, Cairo, 12622, Egypt; [20]Instituto de Genética Médica y Molecular (INGEMM)—IdiPAZ, Hospital Universitario La Paz, Universidad Autónoma, Madrid, 28046, Spain; [21]ITHACA, European Reference Network on Rare Congenital Malformations and Rare Intellectual Disability; [22]Division for Molecular Nutrition, Institute for Basic Medical Sciences, University of Oslo, Oslo, 0316, Norway; [23]Antwerp University Hospital, Edegem, 2650, Belgium; [24]School of Medicine and Menzies Institute for Medical Research, University of Tasmania, Hobart, Tasmania, 7001, Australia; [25]Clinical Genetics Service, Austin Health, Heidelberg, 3084, Victoria, Australia; [26]Department of Chemistry and Biochemistry, University of California, San Diego, 9400 Gilman Drive, La Jolla, CA 92093-0654, USA
[27]These authors contributed equally to this work
[28]These authors contributed equally to this work
*Correspondence: vlruiz@iib.uam.es
https://doi.org/10.1016/j.ajhg.2020.09.005.

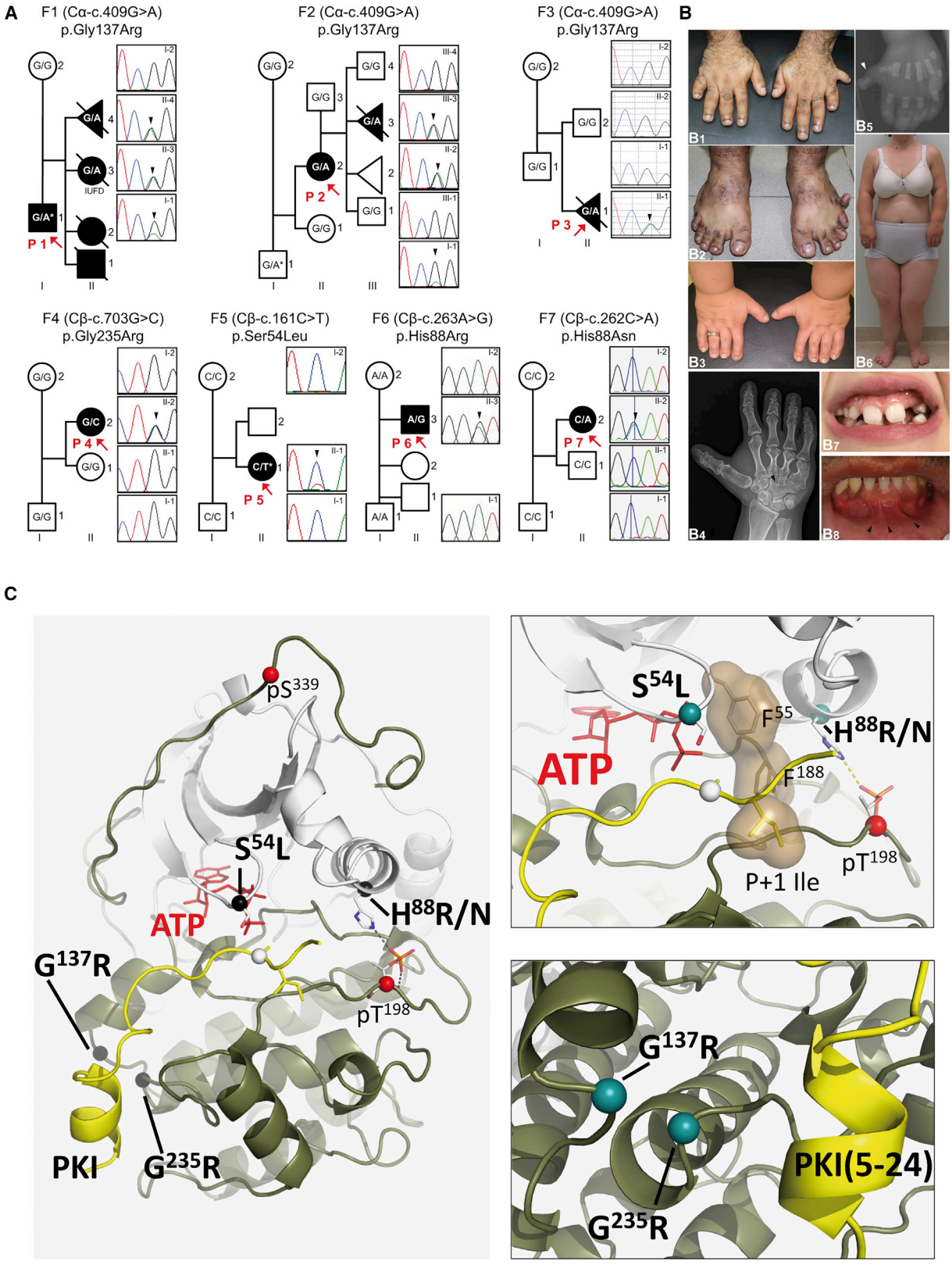

Figure 1. Affected Individuals and Mutations

(A) Family (F) pedigrees of the seven probands (P; red arrows) of this study and DNA sequence electropherograms illustrating mutations (black arrowheads) and their co-segregation with the disease phenotype. Asterisks denote mosaic state of the corresponding mutation in P1, the father of P2 (I-1) and in P5. IUFD: intrauterine fetal death.

(B) Clinical images. Hands and feet of P1 with bilateral postaxial polydactyly and wide sandal gap. The extra digit of the right hand and foot were surgically removed (B1 and B2). Hands of P2 demonstrating brachydactyly and nail dysplasia. Postaxial polydactyly had been

(legend continued on next page)

A-kinase anchoring proteins (AKAPs) and PKA inhibitor proteins (PKI) contribute to PKA subcellular localization and function by binding to R-subunits and C-subunits, respectively.[1]

PKA functions as an intracellular mediator of a variety of G-protein coupled receptor (GPCR) ligands, including specific hormones. Signaling from GPCRs coupled to protein Gαs stimulates adenylate cyclase, leading to increased levels of cAMP and consequently to higher PKA activity. The cAMP/PKA pathway is known to play a central role in the endocrine system because, in addition to mediating the effects of various hormones, it regulates hormone secretion and the proliferation of endocrine cells.[2]

In vertebrates, PKA also works to restrain hedgehog (Hh) signaling through phosphorylation of GLI transcription factors.[3,4] PKA-mediated phosphorylation of full-length GLI3 (GLI3-FL [MIM: 165240]) promotes the conversion of this factor into a strong transcriptional repressor (GLI3R) of Hh-target genes by inducing the proteolytic processing of its C-terminus. GLI3 has a dual function, and uncleaved GLI3FL can be transformed into a transcriptional activator (GLI3A). Hh ligands counteract the activity of PKA by de-repressing the main Hh signal transducer Smoothened (SMO [MIM: 601500]), which is classified as a Frizzled-class GPCR, and recruiting it into the primary cilium. Although the mechanism by which SMO regulates PKA is not fully elucidated, activated SMO suppresses PKA activity, at least partially, by removing from cilia the GPCR GPR161 [MIM: 612250], which presumably operates by increasing the levels of cAMP.[4–6]

PRKACA germline copy number gains have previously been associated with cortisol-producing bilateral adrenal hyperplasias and Cushing's syndrome (CS [MIM: 615830]),[7,8] and *PRKACA* somatic mutations are also found in tumors: cortisol-producing adrenal adenomas of CS individuals, hypothalamic hamartomas, and cardiac myxomas.[7,9,10] Similarly, a *PRKACB* somatic mutation was detected in tumor DNA from a CS individual,[11] and a 1p31.1 triplication encompassing *PRKACB* was described in another individual who had a specific form of Carney complex (CNC [MIM: 160980]) characterized by skin pigmentation, acromegaly, and myxomas, but not CS.[12]

Herein, we studied seven unrelated individuals of different ancestries (P1–P7; Figure 1A–B), all born to non-consanguineous healthy parents, who presented with congenital defects. Two individuals had offspring with the same condition, and the other five were simplex cases. All probands had limb abnormalities consisting of post-axial polydactyly of the hands (6/7 bilateral; 1/7 unilateral) and feet (4/7 bilateral; 1/7 unilateral) and brachydactyly (4/7). Congenital heart defects comprising common atrium or an atrioventricular septal defect (AVSD) were observed in 5/7 individuals. The two probands (P1, P2) without a heart condition had offspring with AVSD. Additionally, short stature/length, short limbs, narrow chest, abnormal teeth, oral frenula, nail dysplasia, and intellectual disability were features present in more than one affected individual. One proband had a history of unusual tumors. Affected individuals were initially diagnosed as having either Ellis-van Creveld syndrome (EvC; MIM: 225500), Weyers acrodental dysostosis (WAD; MIM: 193530), or an undiagnosed syndrome, depending on the presence and severity of chondroectodermal features (Table 1). Serum levels of hormones and bone metabolic markers were assessed in four affected individuals (P1, P2, P4, P7). Endocrine investigations did not show hypercortisolism or an overt endocrine dysfunction. Adrenal imaging in the same four probands (P1, P2, P4, P7) was also negative for adrenal abnormalities. An extended clinical description of the affected individuals is available as Supplemental Information (Supplemental Case Reports). The study was conducted in accordance with the declaration of Helsinki for medical research involving human subjects and was approved by the corresponding institutional ethics committees of the participant institutions. All affected individuals or their legal guardians and family members provided written informed consent for their participation in the study and publication of photographs.

After we excluded mutations in the EvC genes (*EVC* [MIM: 604831 and *EVC2* [MIM: 607261]), we conducted whole-exome sequencing (WES) in families 1 and 2. This analysis identified the same heterozygous missense variant in *PRKACA* (GenBank: NM_002730.4), c.409G>A (p.Gly137Arg), in both unrelated families. Remarkably, this mutation was also found in individual P3. The c.409G>A variant was mosaic in the unaffected father of P2 (variant allele fraction [VAF] = 0.16; altered allele read depth = 508/total read depth = 3,097), and was germline-transmitted in P2 (VAF = 0.55) and her affected offspring (VAF = 0.46). P1 was also mosaic for the same *PRKACA* variant (VAF = 0.28; 811/2,858), and his two affected offspring from whom there was available DNA (II-3 and II-4 in Figure 1A); both carried the variant in the heterozygous state. In P3, the mutation was identified as *de novo*. Next-generation sequencing (NGS) data for the c.409G>A variant and pedigree segregation were confirmed via Sanger sequencing in each family

previously corrected (B3). Radiograph of the right hand of P2 with carpal bone fusion (arrowhead) and brachydactyly (B4). Hand radiograph of III-3 (F2) showing postaxial polydactyly (arrowhead) (B5). Clinical image of P2 demonstrating short stature with short limbs (B6). Diastema and abnormal teeth in P4 at age 9 years (B7). Orodental features of P1 with diastema and multiple lower lingual frenula (arrowheads) (B8).

(C) Sites of mutations in the catalytic subunit of PKA. In the full-length C-subunit (left), the mutations are black spheres. p.Ser54Leu and p.His88Arg/Asn are near the active site (top right, teal spheres) and p.Gly137Arg and p.Gly235Arg (bottom right) are at a tethering surface that interacts with partner proteins, in this case the PKA inhibitor (PKI) peptide (yellow), whose tethering helix docks onto this site.

Table 1. Summary of Clinical and Molecular Findings of Affected Individuals

Clinical features (ethnic origin)	P1 (Egypt)	P2 (Belgium)	P3 (Italy)	P4 (Denmark)	P5 (France)	P6 (France)	P7 (Australia)
Age, gender	33 years, male	42 years, female	fetus (23 weeks), female	18 years, female	15 years, female	20 years, male	41 years, female
Height	165 cm (−1.61 SD)	139 cm (−5 SD); disproportionate short stature	fetus length: 27 cm (<3%)	163 cm (−1 SD)	148.5 cm (−1.8 SD)	175 cm (0 SD)	165 cm (−0.19 SD)
Weight	97 kg (+1.74 SD)	61,5 kg (+0.46 SD)	467 g (25% < p < 50%)	47.3 kg (−2.8 SD)	47 kg (−1 SD)	53 kg (−1.5 SD)	51.2 kg (−1.03 SD)
Head circumference	57 cm (+1.32 SD)	52,6 cm (−1.6 SD)	not available	51 cm (−3 SD)	55 cm (M)	56,5 cm (+ 0.5 SD)	56 cm (+ 1.18 SD)
Congenital heart abnormalities	no, but present in the affected offspring of the proband	no, but present in the affected offspring of the proband	yes, AVSD with myocardial hypertrophy	yes, AVSD and left cava superior entering into the coronary sinus	yes, single atrium, mitral anomaly	yes, single atrium, mild mitral valve regurgitation	yes, single atrium, surgically corrected in infancy; atrial fibrillation in adulthood with persistent incompetence of the valves
Postaxial polydactyly of the hands	yes, bilateral	yes, bilateral	yes, bilateral	yes, bilateral	yes, bilateral	yes, bilateral	yes, unilateral (right hand)
Postaxial polydactyly of the feet	yes, bilateral	no	yes, unilateral (hexadactyly of the left foot)	yes, bilateral	no	yes, bilateral	yes, bilateral
Other hands/ feet anomalies	brachydactyly	brachydactyly; fusion of hamate and capitate in right hand	not reported	short and broad with shortening of middle and distal phalanges and toes	brachydactyly and large great toe	fifth finger clinodactyly (unilateral)	fifth finger clinodactyly, broad toes, and mild digital clubbing
Long trunk	yes	yes, in childhood	not reported	yes	yes, moderate	no	no
Narrow thorax	no, but present in the affected offspring of the proband	yes, in childhood	yes, short ribs	yes	yes, moderate	no	no
Upper/ lower limb shortening	no (arm span 162 cm), but present in the affected offspring of the proband	yes (arm span 121 cm)	micromelia	yes	no	no	no
Genu valgum	yes	yes	not available	yes, genu valgum and previous surgery for coxa vara	yes	no	no, but recurrent dislocated patellae
Teeth abnormalities	yes, congenitally missing upper lateral incisors bilateral and lower right lateral incisor. Diastema	yes, conical teeth; early decay	not available	small central maxillary incisors, conical right canine, and hypodontia, invagination, agenesis, and supernumerary teeth of lateral mandibular incisors	yes, hypodontia	no	no
Nail dysplasia	no, but present in the affected offspring of the proband	yes	not available	yes, especially on the toes, also broad nails on both thumbs	no	no	no

(*Continued on next page*)

Table 1. ***Continued***

Clinical features (ethnic origin)	P1 (Egypt)	P2 (Belgium)	P3 (Italy)	P4 (Denmark)	P5 (France)	P6 (France)	P7 (Australia)
Facial/lip abnormalities	long face with mid face hypoplasia, short philtrum, overhanging nasal tip	notched upper lip	not available	long face, short and deep philtrum, tented upper lip	long face	no	broad forehead, hypertelorism, prognathism, prominent nasal tip
Multiple frenula or abnormal gum-lip attachment	yes, multiple upper and lower lingual frenula, hypoplastic maxilla with cross bite	multiple oral frenula at lower lip present at birth	not available	yes, abnormal gum-lip attachment	multiple oral frenula at lower lip	no	no
Intellectual disability	no	no	not applicable, fetus with brain edema	no, in childhood a period with mild developmental delay including mild language delay, gross motor difficulties, balance problems, and concentration problems; later diagnosed with dyslexia	no	yes, mild intellectual disability, reading and writing acquired, severe anxiety	yes, severe intellectual disability with autistic features. Medically refractory focal epilepsy
Neoplastic lesions	absent at age 33 years	absent at age 42 years	not reported	absent at age 18 years	absent at age 15 years	absent at age 20 years	yes, grade 1 borderline mucinous ovarian tumor, liver haemangioma, renal cell carcinoma
Clinical diagnosis	WAD	EvC	EvC	EvC	EvC	common atrium and polydactyly	common atrium and polydactyly
Affected gene variant description (GRCh37/hg19)	*PRKACA* chr19: 14211648 C>T NM_002730.4: c.409 G>A p.Gly137Arg	*PRKACA* chr19: 14211648 C>T NM_002730.4: c.409 G>A p.Gly137Arg	*PRKACA* chr19: 14211648 C>T NM_002730.4: c.409 G>A p.Gly137Arg	*PRKACB* chr1: 84668426 G>C NM_002731.3: c.703G>C p.Gly235Arg	*PRKACB* Chr1: 84647935 C>T NM_002731.3: c.161C>T p.Ser54Leu	*PRKACB* Chr1: 84649745 A>G NM_002731.3: c.263A>G p.His88Arg	*PRKACB* Chr1: 84649744 C>A NM_002731.3: c.262C>A p.His88Asn
Inheritance	mosaic	inherited	*de novo*	*de novo*	mosaic	*de novo*	*de novo*
NGS; altered allele reads/total read depth	0.28 (811/2,858)[a]	0.55 (41/74)	detected via Sanger sequencing; equal representation of altered and reference alleles in sequencing chromatograms	0.42 (102/239)	0.32 (39/122)	0.54 (20/37)	0.31 (4/13) (the mutant allele was demonstrated to be in the heterozygous state in blood-derived DNA of P7 [~59% mutant allele frequency] and absent in both parents via droplet digital PCR [ddPCR])

(*Continued on next page*)

Table 1. *Continued*

Clinical features (ethnic origin)	P1 (Egypt)	P2 (Belgium)	P3 (Italy)	P4 (Denmark)	P5 (France)	P6 (France)	P7 (Australia)
Other affected family members	yes, two offspring with postaxial polydactyly of both hands, short limbs, and congenital heart septal defects; both died early after birth; an IUFD at 33 weeks of gestation with bilateral postaxial polydactyly and congenital heart disease and a fetus with similar manifestations	yes, one affected fetus with short limbs, narrow thorax, postaxial polydactyly of both hands, and complete AVSD	no	no	no	no	no
Other information		surgery for a lobar emphysema in the left lung at the age of 2 years	the fetus presented with bicornuate and didelphys uterus; lungs with immature parenchyma at canalicular stage were also observed				dural ectasia and osteoporosis with multiple fractures

P: Proband. M: median or 50th percentile. AVSD: atrioventricular septal defect. WAD: Weyers acrodental dysostosis. EvC: Ellis-van Creveld syndrome. IUFD: Intrauterine fetal death. NGS: next-generation sequencing.
[a]To further confirm the mosaic state of the mutation detected by initial standard WES, additional deep WES was carried out in P1. Deep WES was also performed in the father of P2 (altered allele reads (508)/total read depth (3,097) = 0.16).

(Figure 1A, Table 1). Trio-WES in P4, P6, and P7 did not detect changes in *PRKACA* but revealed different *de novo* heterozygous missense variants predicted to be damaging in *PRKACB* (GenBank: NM_002731.3) in the three affected individuals (P4: c.703G>C [p.Gly235Arg], P6: c.263A>G [p.His88Arg], and P7: c.262C>A [p.His88Asn]). WES analysis of P5 also identified a pathogenic change in *PRKACB* (c.161C>T [p.Ser54Leu]). All four *PRKACB* variants were proved to be *de novo* through the use of Sanger sequencing. In P5, the mutation was present in 32% of NGS reads (VAF = 0.32; 39/122) and P5's electropherograms were consistent with this individual also being mosaic (Figure 1A, Table 1). All *PRKACA* and *PRKACB* variants were absent in gnomAD v2.1.1/v3[13] and involved evolutionarily conserved residues (Figure S1). Detailed WES results, including other variants detected and analysis pipelines used, are provided in the Supplemental Information (Figure S2). The p.Ser54Leu variant was previously identified as a somatic mutation in a cortisol-producing adenoma from an individual with CS.[11]

We next confirmed expression of Cα and Cβ transcripts in dermal fibroblasts through the use of RT-PCR (Figure S3A). Sequencing of the resulting RT-PCR fragments demonstrated expression of both normal and mutant *PRKACA* or *PRKACB* alleles in fibroblasts from affected individuals. We also observed the levels and localization of EvC proteins to be similar between cells from control and affected individuals (Figure S3B–S3C). Similarly, localization of PKA-C was found to be unaffected in *PRKACA*- or *PRKACB*-mutant fibroblasts (Figure S3D). In addition, because defects in one PKA subunit can lead to expression changes in other components of the holoenzyme,[14–16] we used qRT-PCR and immunoblotting to study PKA-C and -R expression in dermal fibroblasts. Compared to control cells, fibroblasts from individuals with *PRKACB* mutations showed a slight increase in the mRNA levels of *PRKACA*. PKA-C protein levels were also found to be increased in these cells, although statistical significance was only reached respecting one of the two controls included in the analysis. Furthermore, *PRKACB* mutant cells showed decreased *PRKAR1B* transcript levels. No significant differences, neither at the mRNA nor at the protein levels, of PKA-C or -R subunits were identified in fibroblasts from individuals with the *PRKACA* mutation with respect to controls. Changes in RIIβ protein levels were present in cells from both control and affected individuals and therefore cannot be attributed to the mutations (Figure S3E–S3F).

Analysis of the tertiary structure of the C-subunit revealed that mutations cluster in two groups with Cβ-Ser54 and Cβ-His88 being located in or near the Glycine-rich loop (G-Loop) at the active site and Cα-Gly137 and Cβ-Gly235 in a shared pocket at the end of the D and F helices (Figure 1C). Ensemble models, generated for each mutation, showed that both Cβ-p.His88Arg and Cβ-p.His88Asn altered the dynamics of the G-Loop, predictably affecting synergistic ATP and substrate peptide binding.[17,18] These

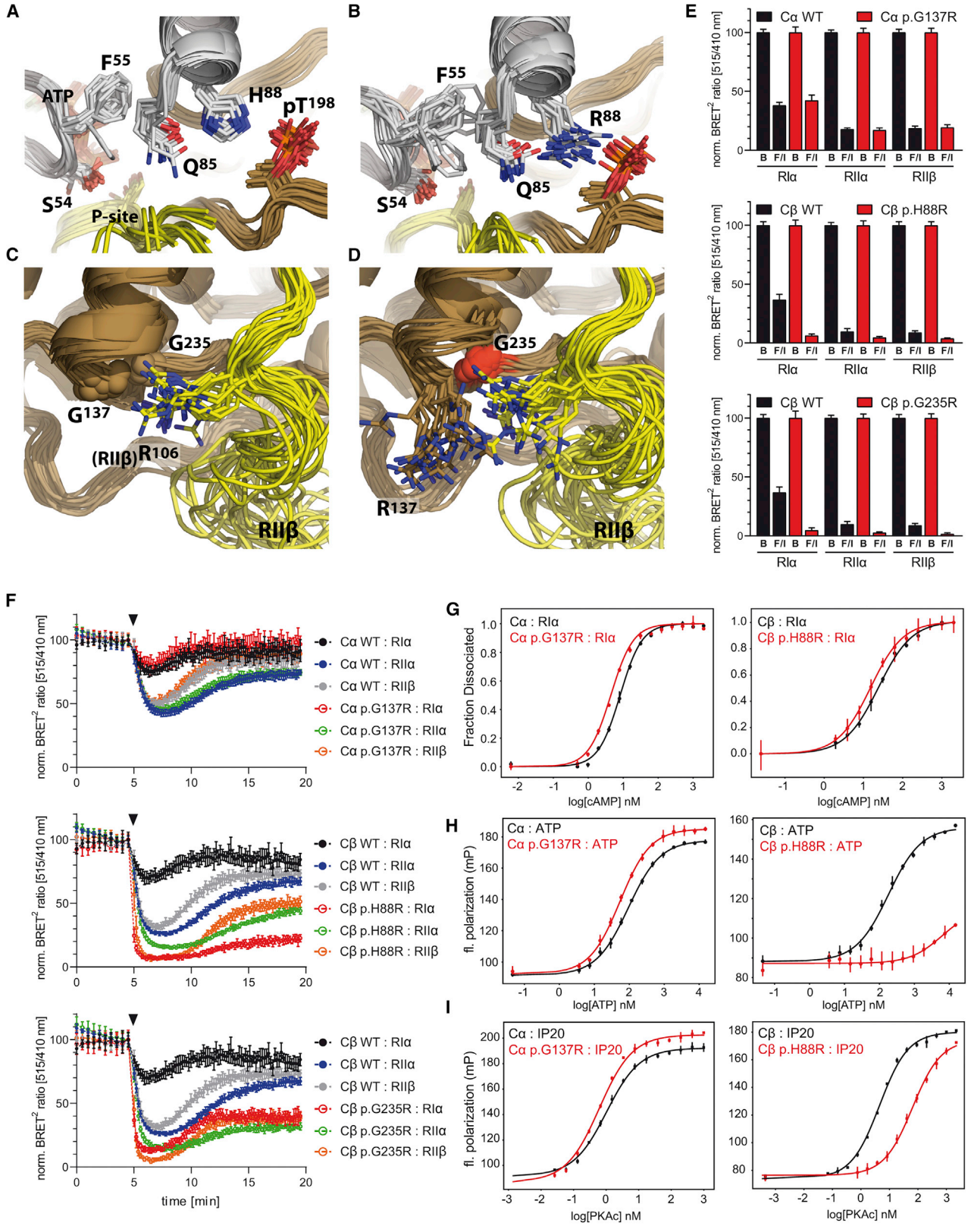

Figure 2. Structural and Functional Assessment of Mutations

(A–D.) Ensemble model of mutations: (A) A stabilizing four-residue network that involves salt bridges between the activation loop phosphate (phospho-Thr198), the C-helix (His88 and Gln85), and hydrophobic packing of Phe55 of the G-Loop onto Gln85 is found in WT PKA. This interaction modulates the conformational dynamics of the G-Loop.

(legend continued on next page)

mutations and the previously described Cβ-p.Ser54Leu[11] likely disrupt ATP-dependent regulation in the G-Loop. Cα-p.Gly137Arg and Cβ-p.Gly235Arg do not affect ATP binding, but they share an interface that forms interactions with regulatory proteins that include PKI, RIα, and RIIβ (Figure 2A–2D and Figure S4).

The effect of the identified mutations in PKA holoenzymes was analyzed by using bioluminescence resonance energy transfer ($BRET^2$), which provides *in cellulae* analysis of holoenzyme dissociation. This study showed a dramatic increase in the sensitivity to cAMP of Cβ-p.His88Arg and Cβ-p.Gly235Arg PKA holoenzymes formed with RIα, RIIα and RIIβ upon Forskolin/IBMX (Figure 2E) or isoproterenol (Figure 2F) stimulation in comparison to the corresponding Cβ-wild-type (Cβ-WT) PKA holoenzymes. Cβ-p.His88Asn showed almost full dissociation upon Forskolin/IBMX (Figure S5A) but a lower response to 100 nM isoproterenol compared to Cβ-p.His88Arg (Figure S5C and Figure 2F). Higher sensitivity to cAMP of the Cβ-p.His88Arg:RIα holoenzyme was additionally demonstrated through the use of fluorescence polarization assays (FPA). Using these assays, we also proved that the reduction in the stability of the Cβ-p.His88Arg:RIα holoenzyme can be attributed to loss of the synergistic effect of ATP binding, which is also true for the PKI peptide (PKI5-24) (Figure 2G–2I; Table S1). In contrast to the Cβ mutations, $BRET^2$ assays showed the dissociation kinetics for Cα-p.Gly137Arg and Cα-WT holoenzymes with RIα, RIIα, and RIIβ to be comparable (Figures 2E-2F). However, using FPA of purified holoenzymes (both RIα and RIIβ), we found greater sensitivity of Cα-p.Gly137Arg to lower cAMP concentration than the wild-type (WT) protein (Figure 2G and Figure S5D). Cα-p.Gly137Arg was additionally characterized with slightly increased cooperative binding for ATP and PKI peptide substrate (Figure 2H–2I; Table S1). Reduced association of Cα-p.Gly137Arg and Cβ-p.Gly235Arg with both RIα and RIIβ compared to their corresponding control C-WT proteins was also observed via co-immunoprecipitation (Figure S5E–S5F). Consistently, the kinase activity of Cα-p.Gly137Arg and Cβ-p.Gly235Arg determined through the use of the PepTag assay, which uses a fluorescent-labeled Kemptide substrate, in extracts from HEK293T co-transfected with both PKA-C and -RIα subunits, was found to be higher than that of their respective WT proteins at low cAMP concentrations (Figure S6).

Subsequently, we assessed the effect of mutations in the Hh pathway by ectopically expressing normal or mutant (Cα-p.Gly137Arg or Cβ-p.Gly235Arg) FLAG-tagged C-subunits together with RIα-GFP in NIH 3T3 via retroviral delivery. Notably, after stimulation of the pathway with the SMO-agonist SAG, the cells that were retrotransduced with the mutant C-subunits showed increased levels of GLI3R and reduced expression of the readout of the Hh pathway GLI1 compared to the control cultures, indicating that both Cα- and Cβ-mutations impair SAG-mediated inactivation of PKA in NIH 3T3 (Figure 3A–3D). Results were similar in cells treated only with FLAG-tagged C-subunit retroviruses (Figure S7). A model explaining the pathological mechanism of C-mutations in Hh signaling is shown in Figure 3E–3G.

In summary, we describe a syndrome involving multiple congenital anomalies caused by germline or mosaic mutations in *PRKACA* or *PRKACB*. Affected individuals had a constellation of features with the major shared findings being common atrium/AVSD and postaxial polydactyly. The association of these two features without other defects was postulated as an independent syndrome in a number of reported affected individuals.[24,25] Common atrium/AVSD and polydactyly are also part of the clinical spectrum of several ciliopathies, and their co-morbidity is often thought to be a consequence of abnormal Hh signaling.[26] Accordingly, germline or mosaic *PRKACA* or *PRKACB* mutations may explain the phenotype in other undiagnosed individuals with common atrium/AVSD-polydactyly alone or as part of more complex phenotypes.

Five of the seven probands in this report (P1–P5) showed phenotypic overlap with EvC or its less-severe dominantly inherited allelic form, WAD.[27] Biallelic loss-of-function

(B) The p.His88Arg (R88) mutation pulls Gln85 away from Phe55 and releases the G-Loop, likely leading to reduced synergistic binding of ATP and reduced affinity for the ATP-dependent RIα subunit. p.Ser54Leu, in the G-Loop, likely similarly affects ATP-dependent regulation by disrupting the G-Loop dynamics.
(C) In WT PKA, a pocket is formed by the D and F helices, and that pocket is accessed in an RIIβ-specific manner by Arg106 in the inhibitor segment (PDB:3TNP) and by the tethering helix in PKI(5-24).
(D) p.Gly137Arg and p.Gly235Arg disturb this RIIβ-specific interaction. This pocket is also at the RIα cAMP-binding domain-B interface (PDB:6NO7) and at the interface with the tethering helix in PKI (Figure S4B–S4C).
(E) In $BRET^2$ experiments, Cα-p.Gly137Arg shows comparable dissociation to that of Cα-WT upon full cAMP-stimulation by Forskolin/IBMX (F/I) for RIα-, RIIα, and RIIβ-holoenzymes, whereas Cβ-p.His88Arg- and Cβ-p.Gly235Arg-holoenzymes fully dissociate. $BRET^2$ data from unstimulated cells treated with buffer only are designated by the letter B. Normalized data are shown as means ± SD of three independent experiments with n = 6 replicates each (total n = 18).
(F) Kinetic $BRET^2$ analyses demonstrate full dissociation upon addition of the physiological β-adrenergic agonist isoproterenol (100 nM, triangle) for Cβ-p.His88Arg and Cβ-p.Gly235Arg and identical behavior of Cα-WT and Cα-p.Gly137Arg. Data shown are means ± SD of n = 6 replicates showing one of three (two for RIIα) independent experiments. For expression levels of GFP-C-subunits used in BRET, see Figure S5B.
(G) FPA analysis: RIα holoenzyme activation by cAMP shows increased sensitivity compared to WT with both Cα-p.Gly137Arg and Cβ-p.His88Arg (n = 3).
(H–I) FPA: Synergistic binding of ATP (H) with PKI 5-24 (IP20) peptide (I) to the C-subunit shows slightly increased binding affinity compared to WT with Cα-p.Gly137Arg and strongly decreased cooperativity with Cβ-p.His88Arg (n = 3). To illustrate differences in total binding, raw fluorescence polarization is expressed as millipolarization units (mP), and otherwise mP has been converted to fraction dissociated. Graphs show the mean ± SD.

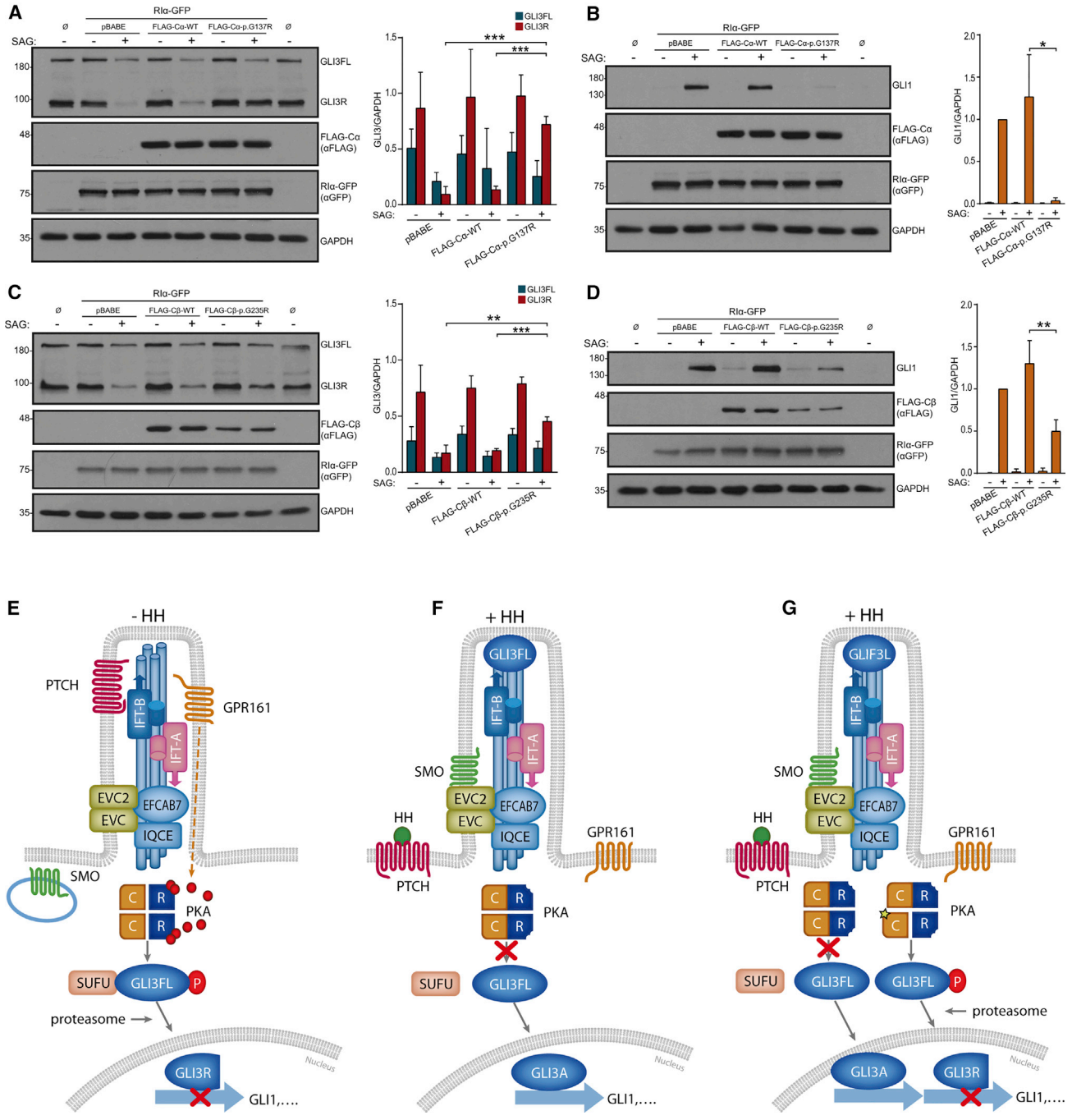

Figure 3. ***PRKACA* and *PRKACB* Mutations Impair Hh Signaling in NIH 3T3**

(A–D) Analysis of GLI3 and GLI1 protein levels in NIH 3T3 co-infected with human FLAG-Cα-WT or FLAG-Cα-p.Gly137Arg and RIα-GFP retroviral vectors (A–B) or alternatively with FLAG-Cβ-WT or FLAG-Cβ-p.Gly235Arg and RIα-GFP retroviruses (C–D), exposed to SAG (+) or its vehicle DMSO (-). Non-infected cells are indicated with Ø. Expression levels of FLAG-C and RIα-GFP are shown in the underneath panels. After incubation with SAG, Cα-p.Gly137Arg and Cβ-p.Gly235Arg retrotransduced cells showed increased GLI3R protein levels and reduced expression of GLI1 compared to cells retrotransduced with pBABE (empty vector) or with FLAG-Cα-WT or FLAG-Cβ-WT. Representative immunoblots are on the left and histograms show densitometric quantification of the levels of GLI3R and GLI3FL referred to GAPDH in (A) and (C), or GLI1/GAPDH levels normalized to the value of SAG-pBABE cells in (B) and (D). Data are expressed as mean ± SD from three experiments corresponding to three independent retroviral infections (n = 3). * = $p < 0.05$; ** = $p < 0.01$; *** = $p < 0.001$. Student's t-test.

(E–G) Model of action of PKA-Cα/β mutations. (E) In the absence of signal, PTCH (the receptor of Hh ligands [HH]) is in the cilium and represses SMO. GPR161 is also located in the cilium membrane and negatively regulates Hh signaling by promoting adenylyl-cyclase-dependent cAMP synthesis (red spheres). Consequently, PKA holoenzymes are active and their C-subunits (C) are free from R-subunits (R) to phosphorylate GLI3FL, which is bound to the inhibitory protein SUFU. Phosphorylated GLI3FL undergoes C-terminal proteolytic processing by the proteasome and is transformed into GLI3R, leading to reduced expression of Hh targets such as GLI1. (F) The

(legend continued on next page)

mutations in *EVC* or *EVC2*, which encode the two subunits of the EvC ciliary complex (EVC and EVC2), are the primary cause of EvC, whereas specific heterozygous C-terminal truncating mutations in *EVC2* are responsible for WAD.[28–30] The EvC complex, which localizes at the base of primary cilia, is required downstream of SMO for complete inhibition of GLI3FL processing in response to Hh ligands.[20–22] Consequently, PKA and EVC-EVC2 act at the same level in the Hh pathway, but in an opposing manner. A scaffolding role for concentrating SMO signaling to the cilium base has been proposed for the EVC-EVC2 complex.[4,21] Given the overlap between EvC/WAD and *PRKACA/B* phenotypes, EVC-EVC2 could specifically link SMO signaling to PKA acting as scaffold, or be involved in a biochemical reaction to prevent the phosphorylation of GLI3 by PKA. Intriguingly, RIα is known to bind specifically to GPR161.[31] The ciliopathy-like phenotype of the individuals of this report is in agreement with the negative effect caused by the identified *PRKACA* and *PRKACB* variants on Hh signaling. However, we cannot rule out the possibility that these mutations could also alter additional molecular pathways regulated by PKA that may be contributing to the phenotype. Skeletal defects have been reported in association with variants in other PKA subunits or other components of cAMP/PKA signaling. Specific variants in *PRKAR1A* lead to acrodysosotosis type 1 (MIM: 101800),[32] and variants in the cAMP phosphodiesterase encoded by *PDE4D* lead to acrodysostosis type 2 (MIM 614613).[33,34] The skeletal phenotype of acrodysostosis (brachydactyly, short stature, facial dysostosis, and nasal hypoplasia) is similar to that of Albright hereditary osteodystrophy and does not typically resemble a ciliopathy. Loss-of-function mutations in *PRKAR1A* resulting in unrestricted PKA activity cause CNC,[35] which is a condition characterized by skin pigmentary abnormalities, endocrine tumors or overactivity, and other tumors such as myxomas or schwannomas. However, polydactyly, common atrium/AVSD, and skeletal and ectodermal defects are not considered to be part of the CNC diagnostic criteria.[36] *Prkar1a*$^{+/-}$ mice have also been shown to be prone to developing bone lesions.[14,15] Considering the individuals reported here, only P7 had tumors, but she did not have evidence of CS, and to date, no adrenal, pituitary, or thyroid tumors have been found on imaging. She did not have the typical skin manifestations of CNC, either. Whether the presence of tumors in P7 is due to the Cβ-p.His88Asn variant needs to be clarified through further investigations. The hormonal profile in the four affected individuals analyzed did not show signs of overt endocrine alterations, and until now, bone tumors have not been identified in any of the affected individuals.

We show that the mutations reported here affect the interaction of C- and R-subunits through an ATP-dependent mechanism (for p.His88Arg, p.His88Asn, and p.Ser54Leu) or through disruption of interfacial surfaces (for p.Gly137Arg and p.Gly235Arg), creating holoenzymes that are more sensitive to cAMP for different reasons. This implies that the mutant Cα- and Cβ-subunits remain more active following the downregulation of cAMP levels associated with Hh signaling,[23] thus decreasing the strength of this pathway. Indeed, diminished Hh signaling activity was observed in NIH 3T3 ectopically expressing mutant C-subunits. Of note, using random mutagenesis in a plasmid containing the mouse Cα subunit, Orellana and McKnight described a p.His87Gln variant (p.His88Gln using our variant nomenclature) that compared to the WT protein retained partial activity in the presence of an excess of RIα subunit.[37]

In our assays, Cα-p.Gly137Arg caused a less severe impact in PKA holoenzymes than the Cβ mutations did. Because Cα is the major PKA C-subunit and is ubiquitously expressed, whereas Cβ is mainly expressed in brain and lymphoid tissues,[38] mutations in Cβ may need to be more damaging than in Cα in order to cause a phenotype in tissues with low Cβ expression. Nonetheless, we cannot discard the possibility that Cα-p.Gly137Arg could also alter an unknown Hh-specific regulatory mechanism of PKA inactivation. During the preparation of this manuscript, we became aware of a large-scale clinical exome sequencing study compiling WES results from >2,200 Saudi families; in this study, the Cα-p.Gly137Arg variant was observed to be *de novo* in one affected individual with clinical suspicion of EvC. The WES result of this individual was stated as ambiguous, and the case was considered not solved because of the unknown causality of the change, which is now demonstrated by our data.[39] This observation further reinforces the recurrent character of the Cα-p.Gly137Arg mutation. While much is known about the Cα-subunit, surprisingly little is known about the Cβ-subunit. Our discovery of these mutations underscores the need to now distinguish between the structural and functional differences of Cβ splice variants that remain as an

interaction of Hh ligands with PTCH disables this protein to continue repressing SMO and PTCH-HH complexes exit from cilia. Derepressed SMO accumulates into the cilium and interacts with the EvC ciliary complex, which is retained at the base of this organelle through binding of the C-terminal of EVC2 to the EFCAB7-IQCE complex.[19] In this manner, SMO signaling is enriched at the EvC region. SMO and the EvC proteins promote GLI3FL-SUFU dissociation and stimulate the recruitment of GLI3 to cilia tips.[20–22] Active SMO additionally causes GPR161 to abandon the cilium, and this, in combination with other not fully understood SMO-mediated mechanisms, results in decreased levels of cAMP and the inactivation of PKA.[4,23] Accordingly, GLI3FL phosphorylation is stopped and the production of GLI3R discontinued while GLI3FL is converted into a functional transcriptional activator (GLI3A). (G) The same situation as in (F), but in an individual with a *PRKACA* or *PRKACB* mutation. Due to higher cAMP sensitivity of the mutant PKA holoenzymes, the mutant PKA C-subunits (star) remain active following downregulation of cAMP levels associated with the activation of the Hh pathway, thus leading to abnormally increased levels of GLI3R and reduced Hh pathway activity. Affected individuals are expected to have holoenzymes containing two normal or two mutant C-subunits and holoenzymes composed of one normal and one mutant C-subunit. Intraflagellar transport protein complexes (IFT-A and IFT-B) which are also involved in Hh signaling are indicated in (E–G).

unexplored frontier. Our findings demonstrate a critical role of both Cα- and Cβ-subunits of PKA in human development.

Data and Code Availability

Specific datasets supporting this article or additional information not subjected to ethical restrictions can be obtained from the corresponding author upon request.

Supplemental Data

Supplemental Data can be found online at https://doi.org/10.1016/j.ajhg.2020.09.005.

Acknowledgments

We thank all affected individuals, their siblings, and their parents or legal guardians for their participation in this study. Some individuals were included after a GeneMatcher match.[40] This work was partially supported by funding from the Spanish Ministry of Science, Innovation and Universities (SAF2016-75434-R [AEI/FEDER, UE] and PID2019-105620RB-I00/AEI/10.13039/501100011033) to V.L.R.-P. S.S.T. was supported by NIH grant R03TR002947, E.M.F.M. by Kassel graduate school "Clocks", and A.D.L. by the Italian Ministry of Health (RC-2019). The University of Antwerp supported G.M. and W.V.H. with Methusalem funding (FFB190208) and S.P. with a predoctoral grant. E.B. was supported by The Research Foundation Flanders with a postdoctoral grant (12A3814N). The study was also funded by a National Health and Medical Research Council Program Grant (1091593) to I.E.S., a Practitioner Fellowship (1006110) to I.E.S., a Senior Research Fellowship (1102971) to M.B., and an R.D. Wright Career Development Fellowship (1063799) to M.S.H. B.S.S. and G.L. were supported by Throne Holst Foundation UiO (2019-2021) and Strategic PhD fund by UiO/IMB.

Declaration of Interests

I.E.S has served on scientific advisory boards for UCB, Eisai, GlaxoSmithKline, BioMarin, Nutricia, and Xenon Pharmaceuticals and on editorial boards of the Annals of Neurology, Neurology and Epileptic Disorders; may accrue future revenue on pending patent WO61/010176 (filed: 2008): Therapeutic Compound, a patent for SCN1A testing held by Bionomics Inc. and licensed to various diagnostic companies; has received speaker honoraria from GlaxoSmithKline, Athena Diagnostics, UCB, BioMarin, Biocodex, Eisai, and Transgenomics; and has received funding for travel from Athena Diagnostics, UCB, Biocodex, GlaxoSmithKline, Biomarin, and Eisai. The remaining authors declare no competing interests.

Received: April 28, 2020
Accepted: September 9, 2020
Published: October 14, 2020

Web Resources

ClinVar, https://www.ncbi.nlm.nih.gov/clinvar/
dbSNP, https://www.ncbi.nlm.nih.gov/snp/
gnomAD Browser, https://gnomad.broadinstitute.org/
OMIM, https://www.omim.org/
UCSC Genome Browser, https://genome.ucsc.edu/

References

1. Søberg, K., and Skålhegg, B.S. (2018). The Molecular Basis for Specificity at the Level of the Protein Kinase a Catalytic Subunit. Front. Endocrinol. (Lausanne) *9*, 538.
2. Peverelli, E., Mantovani, G., Lania, A.G., and Spada, A. (2013). cAMP in the pituitary: an old messenger for multiple signals. J. Mol. Endocrinol. *52*, R67–R77.
3. Huang, Y., Roelink, H., and McKnight, G.S. (2002). Protein kinase A deficiency causes axially localized neural tube defects in mice. J. Biol. Chem. *277*, 19889–19896.
4. Kong, J.H., Siebold, C., and Rohatgi, R. (2019). Biochemical mechanisms of vertebrate hedgehog signaling. Development *146*, dev166892. https://doi.org/10.1242/dev.166892.
5. Mukhopadhyay, S., Wen, X., Ratti, N., Loktev, A., Rangell, L., Scales, S.J., and Jackson, P.K. (2013). The ciliary G-protein-coupled receptor Gpr161 negatively regulates the Sonic hedgehog pathway via cAMP signaling. Cell *152*, 210–223.
6. Nachury, M.V., and Mick, D.U. (2019). Establishing and regulating the composition of cilia for signal transduction. Nat. Rev. Mol. Cell Biol. *20*, 389–405.
7. Beuschlein, F., Fassnacht, M., Assié, G., Calebiro, D., Stratakis, C.A., Osswald, A., Ronchi, C.L., Wieland, T., Sbiera, S., Faucz, F.R., et al. (2014). Constitutive activation of PKA catalytic subunit in adrenal Cushing's syndrome. N. Engl. J. Med. *370*, 1019–1028.
8. Carney, J.A., Lyssikatos, C., Lodish, M.B., and Stratakis, C.A. (2015). Germline PRKACA amplification leads to Cushing syndrome caused by 3 adrenocortical pathologic phenotypes. Hum. Pathol. *46*, 40–49.
9. Hildebrand, M.S., Griffin, N.G., Damiano, J.A., Cops, E.J., Burgess, R., Ozturk, E., Jones, N.C., Leventer, R.J., Freeman, J.L., Harvey, A.S., et al. (2016). Mutations of the Sonic Hedgehog Pathway Underlie Hypothalamic Hamartoma with Gelastic Epilepsy. Am. J. Hum. Genet. *99*, 423–429.
10. Tseng, I.C., Huang, W.J., Jhuang, Y.L., Chang, Y.Y., Hsu, H.P., and Jeng, Y.M. (2017). Microinsertions in PRKACA cause activation of the protein kinase A pathway in cardiac myxoma. J. Pathol. *242*, 134–139.
11. Espiard, S., Knape, M.J., Bathon, K., Assié, G., Rizk-Rabin, M., Faillot, S., Luscap-Rondof, W., Abid, D., Guignat, L., Calebiro, D., et al. (2018). Activating PRKACB somatic mutation in cortisol-producing adenomas. JCI Insight *3*, e98296. https://doi.org/10.1172/jci.insight.98296.
12. Forlino, A., Vetro, A., Garavelli, L., Ciccone, R., London, E., Stratakis, C.A., and Zuffardi, O. (2014). PRKACB and Carney complex. N. Engl. J. Med. *370*, 1065–1067.
13. Karczewski, K.J.J., Francioli, L.C., Tiao, G., Cummings, B.B., Alföldi, J., Wang, Q., Collins, R.L., Laricchia, K.M., Ganna, A., Birnbaum, D.P., et al. (2019). Variation across 141,456 human exomes and genomes reveals the spectrum of loss-of-function intolerance across human protein-coding genes. bioRxiv. https://doi.org/10.1101/531210.
14. Liu, S., Saloustros, E., Mertz, E.L., Tsang, K., Starost, M.F., Salpea, P., Faucz, F.R., Szarek, E., Nesterova, M., Leikin, S., and Stratakis, C.A. (2015). Haploinsufficiency for either one of the type-II regulatory subunits of protein kinase A improves the bone phenotype of Prkar1a+/- mice. Hum. Mol. Genet. *24*, 6080–6092.
15. Tsang, K.M., Starost, M.F., Nesterova, M., Boikos, S.A., Watkins, T., Almeida, M.Q., Harran, M., Li, A., Collins, M.T., Cheadle, C., et al. (2010). Alternate protein kinase A activity

identifies a unique population of stromal cells in adult bone. Proc. Natl. Acad. Sci. USA *107*, 8683–8688.
16. Yin, Z., Pringle, D.R., Jones, G.N., Kelly, K.M., and Kirschner, L.S. (2011). Differential role of PKA catalytic subunits in mediating phenotypes caused by knockout of the Carney complex gene Prkar1a. Mol. Endocrinol. *25*, 1786–1793.
17. Taylor, S.S., Yang, J., Wu, J., Haste, N.M., Radzio-Andzelm, E., and Anand, G. (2004). PKA: a portrait of protein kinase dynamics. Biochim. Biophys. Acta *1697*, 259–269.
18. Lew, J., Coruh, N., Tsigelny, I., Garrod, S., and Taylor, S.S. (1997). Synergistic binding of nucleotides and inhibitors to cAMP-dependent protein kinase examined by acrylodan fluorescence spectroscopy. J. Biol. Chem. *272*, 1507–1513.
19. Pusapati, G.V., Hughes, C.E., Dorn, K.V., Zhang, D., Sugianto, P., Aravind, L., and Rohatgi, R. (2014). EFCAB7 and IQCE regulate hedgehog signaling by tethering the EVC-EVC2 complex to the base of primary cilia. Dev. Cell *28*, 483–496.
20. Caparrós-Martín, J.A., Valencia, M., Reytor, E., Pacheco, M., Fernandez, M., Perez-Aytes, A., Gean, E., Lapunzina, P., Peters, H., Goodship, J.A., and Ruiz-Perez, V.L. (2013). The ciliary Evc/Evc2 complex interacts with Smo and controls Hedgehog pathway activity in chondrocytes by regulating Sufu/Gli3 dissociation and Gli3 trafficking in primary cilia. Hum. Mol. Genet. *22*, 124–139.
21. Dorn, K.V., Hughes, C.E., and Rohatgi, R. (2012). A Smoothened-Evc2 complex transduces the Hedgehog signal at primary cilia. Dev. Cell *23*, 823–835.
22. Yang, C., Chen, W., Chen, Y., and Jiang, J. (2012). Smoothened transduces Hedgehog signal by forming a complex with Evc/Evc2. Cell Res. *22*, 1593–1604.
23. Moore, B.S., Stepanchick, A.N., Tewson, P.H., Hartle, C.M., Zhang, J., Quinn, A.M., Hughes, T.E., and Mirshahi, T. (2016). Cilia have high cAMP levels that are inhibited by Sonic Hedgehog-regulated calcium dynamics. Proc. Natl. Acad. Sci. USA *113*, 13069–13074.
24. Levin, S.E., Dansky, R., Milner, S., Benatar, A., Govendrageloo, K., and du Plessis, J. (1995). Atrioventricular septal defect and type A postaxial polydactyly without other major associated anomalies: a specific association. Pediatr. Cardiol. *16*, 242–246.
25. Onat, T. (1994). Post-axial hexodactily and single atrium: a new syndrome? Hum. Genet. *94*, 104–106.
26. Digilio, M.C., Pugnaloni, F., De Luca, A., Calcagni, G., Baban, A., Dentici, M.L., Versacci, P., Dallapiccola, B., Tartaglia, M., and Marino, B. (2019). Atrioventricular canal defect and genetic syndromes: The unifying role of sonic hedgehog. Clin. Genet. *95*, 268–276.
27. Ruiz-Perez, V.L., and Goodship, J.A. (2009). Ellis-van Creveld syndrome and Weyers acrodental dysostosis are caused by cilia-mediated diminished response to hedgehog ligands. Am. J. Med. Genet. C. Semin. Med. Genet. *151C*, 341–351.
28. Ruiz-Perez, V.L., Ide, S.E., Strom, T.M., Lorenz, B., Wilson, D., Woods, K., King, L., Francomano, C., Freisinger, P., Spranger, S., et al. (2000). Mutations in a new gene in Ellis-van Creveld syndrome and Weyers acrodental dysostosis. Nat. Genet. *24*, 283–286.
29. Ruiz-Perez, V.L., Tompson, S.W., Blair, H.J., Espinoza-Valdez, C., Lapunzina, P., Silva, E.O., Hamel, B., Gibbs, J.L., Young, I.D., Wright, M.J., and Goodship, J.A. (2003). Mutations in two nonhomologous genes in a head-to-head configuration cause Ellis-van Creveld syndrome. Am. J. Hum. Genet. *72*, 728–732.
30. Valencia, M., Lapunzina, P., Lim, D., Zannolli, R., Bartholdi, D., Wollnik, B., Al-Ajlouni, O., Eid, S.S., Cox, H., Buoni, S., et al. (2009). Widening the mutation spectrum of EVC and EVC2: ectopic expression of Weyer variants in NIH 3T3 fibroblasts disrupts Hedgehog signaling. Hum. Mutat. *30*, 1667–1675.
31. Bachmann, V.A., Mayrhofer, J.E., Ilouz, R., Tschaikner, P., Raffeiner, P., Röck, R., Courcelles, M., Apelt, F., Lu, T.W., Baillie, G.S., et al. (2016). Gpr161 anchoring of PKA consolidates GPCR and cAMP signaling. Proc. Natl. Acad. Sci. USA *113*, 7786–7791.
32. Linglart, A., Menguy, C., Couvineau, A., Auzan, C., Gunes, Y., Cancel, M., Motte, E., Pinto, G., Chanson, P., Bougnères, P., et al. (2011). Recurrent PRKAR1A mutation in acrodysostosis with hormone resistance. N. Engl. J. Med. *364*, 2218–2226.
33. Lee, H., Graham, J.M., Jr., Rimoin, D.L., Lachman, R.S., Krejci, P., Tompson, S.W., Nelson, S.F., Krakow, D., and Cohn, D.H. (2012). Exome sequencing identifies PDE4D mutations in acrodysostosis. Am. J. Hum. Genet. *90*, 746–751.
34. Michot, C., Le Goff, C., Goldenberg, A., Abhyankar, A., Klein, C., Kinning, E., Guerrot, A.M., Flahaut, P., Duncombe, A., Baujat, G., et al. (2012). Exome sequencing identifies PDE4D mutations as another cause of acrodysostosis. Am. J. Hum. Genet. *90*, 740–745.
35. Kirschner, L.S., Carney, J.A., Pack, S.D., Taymans, S.E., Giatzakis, C., Cho, Y.S., Cho-Chung, Y.S., and Stratakis, C.A. (2000). Mutations of the gene encoding the protein kinase A type I-alpha regulatory subunit in patients with the Carney complex. Nat. Genet. *26*, 89–92.
36. Mateus, C., Palangié, A., Franck, N., Groussin, L., Bertagna, X., Avril, M.F., Bertherat, J., and Dupin, N. (2008). Heterogeneity of skin manifestations in patients with Carney complex. J. Am. Acad. Dermatol. *59*, 801–810.
37. Orellana, S.A., and McKnight, G.S. (1992). Mutations in the catalytic subunit of cAMP-dependent protein kinase result in unregulated biological activity. Proc. Natl. Acad. Sci. USA *89*, 4726–4730.
38. Cadd, G., and McKnight, G.S. (1989). Distinct patterns of cAMP-dependent protein kinase gene expression in mouse brain. Neuron *3*, 71–79.
39. Monies, D., Abouelhoda, M., Assoum, M., Moghrabi, N., Rafiullah, R., Almontashiri, N., Alowain, M., Alzaidan, H., Alsayed, M., Subhani, S., et al. (2019). Lessons Learned from Large-Scale, First-Tier Clinical Exome Sequencing in a Highly Consanguineous Population. Am. J. Hum. Genet. *104*, 1182–1201.
40. Sobreira, N., Schiettecatte, F., Valle, D., and Hamosh, A. (2015). GeneMatcher: a matching tool for connecting investigators with an interest in the same gene. Hum. Mutat. *36*, 928–930.

The American Journal of Human Genetics, Volume *107*

Supplemental Data

Germline and Mosaic Variants in *PRKACA* and *PRKACB* Cause a Multiple Congenital Malformation Syndrome

Adrian Palencia-Campos, Phillip C. Aoto, Erik M.F. Machal, Ana Rivera-Barahona, Patricia Soto-Bielicka, Daniela Bertinetti, Blaine Baker, Lily Vu, Francesca Piceci-Sparascio, Isabella Torrente, Eveline Boudin, Silke Peeters, Wim Van Hul, Celine Huber, Dominique Bonneau, Michael S. Hildebrand, Matthew Coleman, Melanie Bahlo, Mark F. Bennett, Amy L. Schneider, Ingrid E. Scheffer, Maria Kibæk, Britta S. Kristiansen, Mahmoud Y. Issa, Mennat I. Mehrez, Samira Ismail, Jair Tenorio, Gaoyang Li, Bjørn Steen Skålhegg, Ghada A. Otaify, Samia Temtamy, Mona Aglan, Aia E. Jønch, Alessandro De Luca, Geert Mortier, Valérie Cormier-Daire, Alban Ziegler, Mathew Wallis, Pablo Lapunzina, Friedrich W. Herberg, Susan S. Taylor, and Victor L. Ruiz-Perez

Supplemental Case Reports

Family 1. The proband is a 33-year-old Egyptian male who presented with postaxial polydactyly and history of two previous offspring deaths from a non-consanguineous marriage, both had short limbs, postaxial polydactyly and congenital heart disease.

The first pregnancy was a boy delivered at full term by caesarean section (CS). This baby had postaxial polydactyly in both hands, short limbs, nail dystrophy and congenital heart defect. Respiratory distress and meconium aspiration at birth needed incubation and mechanical ventilation. The boy died at 17 days from respiratory failure. The second pregnancy was a girl born at full term by CS. She had the same manifestations of her brother and was incubated for 4 days. Echocardiography at 4 months of age revealed atrioventricular canal (AVC) with common atrium, atrial septal defect measuring 2 cm. The left atrium was relatively small with small mitral valve annulus. There was subaortic ventricular septal defect (VSD) measuring 0.25 cm with no apparent flow because of severe pulmonary hypertension (PHTN). There was prolapse of anterior mitral leaflet with subsequent mitral regurgitation (MR III) and peak velocity 3.5 m/sec and she died at 4.5 months from cardiac and respiratory failure.

Examination of the proband revealed a stocky body built, relatively long trunk and generalized hirsutism. He has long face with mid face hypoplasia, prominent nose, overhanging nasal tip, short philtrum and short neck. Orodental assessment revealed asymmetry of face, hypoplastic maxilla, short lingual frenum, multiple upper and lower lingual frenula, diastema, crossbite, congenitally missing upper lateral incisors, bilateral, and lower right lateral incisor. His height was 165 cm (- 1.61 SD) with arm span of 162.2 cm, weight was 97 kg (+ 1.74 SD) and head circumference of 57 cm (+ 1.32 SD). Examination of limbs showed postaxial polydactyly of both hands and feet (surgical removal of the extra digit was performed on the right hand and foot) and wide space between big toe and second toe in both feet. His nails were normal. Echocardiography was done for screening and it was normal. His wife was normal at time of first presentation to the clinic.

Abdominal ultrasound (US) conducted in the proband at age 33 years was found normal apart from fatty liver. No suprarenal abnormalities were detected by US. The following endocrinology lab tests were also performed at the same age (reference values are indicated between brackets): serum calcium: 9.5 mg/dL (8.5-10.2), serum phosphorous: 4 mg/dL (2.5-4.5), TSH: 4.65 uIU/mL (0.55-4.78), FT4: 1.2 ng/dL (0.8-1.8), Prolactin: 20.4 ng/mL (4-15.2),Testosterone-total: 2.86 ng/mL (2.6-10), Cortisol –am: 10.53 ug/dL (6.2-19.4), ACTH –am: 20.15pg/mL (7.2-63.3), Growth hormone

(basal): 0.03 ng/mL (0.03-2.47), insulin like growth factor 1 (IGF1): 173 ng/mL (43-209), Parathyroid hormone (PTH): 63 pg/mL (15-65), and 25 OH vitamin D: 10.32 ng/mL (deficient <20). All lab results were normal except prolactin that was mildly elevated and vitamin D low. However, this man does not have any manifestations of hyperprolactinemia (no headache, no gynecomastia, no fertility problems, normal testosterone, normal liver and kidney functions) and by history he did not receive any medications for hypertension, gastroesophageal reflux, nausea, vomiting, depression or antipsychotics that may elevate prolactin levels. Hyperprolactinemia is usually defined as fasting levels of above 20 ng/mL in men and above 25 ng/mL in women. Prolactinoma is likely if prolactin levels are greater than 250 ng/mL. Follow up was scheduled to ensure whether this is persistent hyperprolactinemia or a transient event. He had low 25 OH vitamin D, but serum calcium and PTH were normal. He has started oral treatment with vitamin D3.

After examination of the proband, the couple had a third pregnancy that resulted in an affected girl with similar clinical manifestations as the previous siblings. This girl died intrauterine at 33 weeks of gestation due to wrapped cord around the neck with true knot of the cord. She was delivered by CS and the skin was macerated. Another following pregnancy was terminated at 16 weeks of gestation because of a similarly affected fetus with congenital heart disease in the form of single ventricle and abnormalities of great vessels, short long bones and postaxial polydactyly. Samples were taken from both fetuses for molecular studies.

Family 2. The proband is a 42-year-old female born to non-consanguineous and healthy parents of Belgian origin. She was born at term with a birth weight of 3100 g, length of 46 cm and head circumference of 34 cm. She presented after birth with postaxial hexadactyly of both hands, narrow thorax, short limbs and nail dysplasia on fingers and toes. Multiple oral frenula were also visible in the mouth. At the age of 2 months she underwent a lobectomy because of emphysema in the upper lobe of the left lung. At 20 months of age the extra fingers were surgically removed. Clinical evaluation at the age of 35 years revealed disproportionate short stature with a height of 139 cm (- 5 SD) and an arm span of 121 cm. She had short limbs with significant brachydactyly of hands and feet and nail dysplasia on fingers and toes. Her weight was 61.5 kg (+ 0.46 SD) and head circumference was 52.6 cm (- 1.6 SD). The thorax was not narrow. She had bilateral cubitus valgus and genua valga. In the mouth, no frenula were found. She had multiple dental crowns. She gave birth to two healthy sons. The second pregnancy resulted in a miscarriage. The third pregnancy was terminated at 24 weeks. Ultrasound evaluation of the female fetus revealed short limbs, narrow thorax,

congenital heart defect and postaxial polydactyly on both hands. Postmortem examination confirmed the presence of short limbs, postaxial hexadactyly of both hands, short ribs and complete atrioventricular septal defect of the heart.

Recent endocrine investigations in this proband showed test values within the normal range. Serum calcium: 2.40 mmol/L (2.18-2.60), serum phosphate: 1.19 mmol/L (0.78-1.65), calcium phosphate: 3.0 $mmol^2/L^2$ (<4.0), TSH: 1.20 mU/L (0.55-4.78), FT4 free: 16.4 pmol/L (11.5-22.7), Prolactine: 8.2 µg/L (2.8-29.2), Growth hormone: 2.6µg/L, IGF1: 181ng/mL (76-234), PTH (1-84): 26 ng/L (18.5-88.0), 25-OH vitamin D: 27ng/mL (9-48), ACTH: 22 pg/mL (7-63), cortisol –am: 105.0 ng/mL. Ultrasound of kidneys and suprarenal glands revealed no abnormalities.

Family 3. The proband was a female fetus suspected of having Ellis-van Creveld syndrome based on ultrasonographic imaging findings. She was the first pregnancy of healthy non-consanguineous parents of Italian origin. Due to fetal anomalies, the pregnancy was terminated at 23 weeks of gestation and a fetal autopsy was performed. Fetus length and weight were 27 cm (<3%) and 467 g (25%<p<50%), respectively. Radiological evaluation revealed micromelia, short ribs and narrow thorax. Examination of limbs showed postaxial hexadactyly of both hands and of the left foot. Echocardiography highlighted the presence of atrioventricular canal defect with myocardial hypertrophy. Histological assessment pointed out both lungs with immature parenchyma at canalicular stage, meanwhile renal, hepatic and pancreatic parenchyma were normal, thus excluding hepato-renal-pancreatic dysplasia. Moreover, the fetus presented with cerebral edema and genitourinary malformation, specifically, a bicornuate and didelphys uterus was observed. Given the earliness of the observation, the possible ectodermal dysplasia could not be evaluated. The family had a second son. He was born healthy, and referred healthy at 2 years of age.

Family 4. Proband 4 is an 18-year-old female, the 2nd child of healthy non-consanguineous parents. She was born at 40 weeks and 2 days of gestation with a birth weight of 3660 g, birth length 54 cm, and head circumference 35 cm. She was born with bilateral postaxial polydactyly of hands and feet, that was surgically corrected at 9 months of age. At the time of surgery, a congenital heart defect was detected due to a low oxygen saturation (90%) and arrhythmias. Echocardiogram showed partial AVSD (ASD type 1 ostium primum defect) and left cava superior entering into the coronary sinus, considered a rare anatomic variant that was surgically corrected at the age of 14 months. After successful heart surgery she had, as expected, a slight mitral valve insufficiency, without hemodynamic importance, notable as a grade 1 systolic

murmur at the left sternal border/apex. At the age of six years, she had hip surgery performed due to coxa vara (bilateral intertrochanteric osteotomy).

This girl is generally healthy. She had a single episode of febrile seizure at the age of two years. At the age of 12 years she needed glasses to correct for myopia. Her hearing is normal. General physical examination revealed mild disproportionate short stature with shortening of both upper and lower limbs. She is currently 163 cm (- 1 SD), weight 47.3 kg (- 2.8 SD) and has a head circumference of 51 cm (- 3 SD). Parental heights are 176.3 cm and 176.1 cm, respectively. She presents a long and narrow thorax, bilateral genu valga and mild cubitus varus. Hands and feet are short and broad with shortening of middle and distal phalanges and toes (current shoe size 35). Further broadening of distal phalanges 2 to 5, and first fingers and toes are noted. The girl is only able to hold a pencil for a short period of time.

Nails are dysplastic especially on the toes, and broad on first finger bilaterally. The hair was fine but not sparse. Mild facial dysmorphism including a long facial appearance and neck, a broad chin and nose as well as a short and deep philtrum was noticed. The upper lip is tented and nasolabial folds are underdeveloped. Ears are low set and small with small lobes and prominent superior crus. Intraoral examination revealed small maxillary central incisors and a conical right canine, as well as hypodontia, invagination, agenesis and supernumerary teeth of mandibular lateral incisors. Oral frenula are not present, but fusion of parts of the upper and lower lip to the maxillary and mandibular gingival mucosa was noted. She is currently wearing bracelets on upper and lower teeth as part of her dental care.

A developmental evaluation, which took place when the girl was approximately 4 ½ years, revealed mild language delay, gross motor difficulties and balance problems as well as concentration problems and a developmental level of 3 to 3.9 years using the Psychoeducational Profile Revised (PEP-R) and the Wechsler Preschool and Primary Scale of Intelligence-Revised (WPPSI-R), respectively. To improve development, she received physiotherapy and part-time pedagogical support as well as exercise at home. She went through an ordinary school program, and she now attends an ordinary high school program. She was diagnosed with dyslexia at the age of 11 years, and she used a special computer developed for dyslexic individuals for her schoolwork. Due to later unremarkable development no formal cognitive assessments have been carried out at older age.

X-ray of hands and feet before surgical removal of the extra-digits at the age of 9 months had shown a 6th rudimentary finger bilaterally with rudimentary metacarpal

bones and proximal phalanges. Middle and distal phalanges were not visible. In addition, the right 5th metacarpal bone was irregular and broad. Bilateral complete 6th toes with presence of metatarsal bones and phalanges were also observed. X-ray of hands and feet was repeated at age three years. Right hand showed some signs of the previously surgically corrected polydactyly on the 5th metacarpal bone. All metacarpal bones were short and slightly plumb. The middle phalanges were short and wide with "bell shaped" epiphyses and hypoplasia of distal phalanges was also present. The shape and size of the proximal phalanges were normal. Both feet were broad with short metatarsal bones. Anteroposterior (AP) X-ray view of upper and lower limbs, also at the age of three, showed the length of ulna, radius, and the long bones of the lower limbs (femur, tibia and fibula) mildly shortened. The clinical findings were suggestive of Ellis-van Creveld syndrome and she was seen regularly during childhood at the Departments of Orthopedics, Pediatrics and Cardiology as well as the Dentist.

Endocrine investigations performed at current age showed serum levels of hormones generally normal. Cortisol–am (8:30 am): 433 nmol/L (reference 200-700), ACTH: 2.5 pmol/L (1.6-14), PTH: 5.7 pmol/L (1.6-6.0), somatotropin (GH): 0.81 µg/L, IGF1: 381 µg/L (149-459) and TSH: 1.2 mIU/L (0.50-4.3). Serum levels of calcium: 1.25 mmol/L (1.18-1.32), phosphate: 1.33 mmol/L (0.76-1.41) and 25-hydroxy vitamin D: 64 nmol/L (50-160) were also normal. Recent abdominal MRI scan of this proband revealed no adrenal lesions.

Family 5. The proband is a girl, first child of healthy parents. She was born at 39 weeks with a birth weight of 2600 g, birth length 48 cm and head circumference 35 cm. She presented with bilateral postaxial polydactyly of both hands and multiple oral frenula. Echocardiogram detected an atrioventricular septal defect with single atrium and mitral anomaly and she had open-heart surgery to repair. She had a long and narrow thorax and abnormal teeth (hypodontia). She had a normal development. At 14 years of age, her height was at 148.5 cm (- 1.8 SD) and weight 41 Kg (- 1 SD). The girl presented a long and narrow thorax and bilateral genu valga. Hands and feet were short and broad with shortening of middle and distal phalanges of toes (shoe size 33). She had also some degree of hyperlaxity.

Family 6. Proband 6 is a male, the third child of an unrelated couple of French origin. The family history is remarkable for a single atrium in a paternal cousin of the proband. He was born with a single atrium and postaxial polydactyly of all four limbs requiring surgery. Following this surgery, he developed localized myoclonus (upper limb) consecutive to an ischemic stroke. These seizures were efficiently treated with

carbamazepine until the age of two years. MRI brain performed at one year of age for this stroke did not reveal any associated malformations.

Independent walking was acquired at the age of 30 months. Growth is normal (at 20 years: height 175 cm (M), weight 53 kg (- 1.5 SD) and OFC 56.5 cm (+ 0.5SD)). The acquisition of speech has been slightly delayed. At the last examination, he was perfectly able to communicate despite a fluctuating stuttering. A specialized education has enabled the boy to acquire reading and writing. He was autonomous (living in his own apartment and working as an Interim employee). Routine abdominal ultrasound at age 20 years was normal.

Family 7. The proband is a 41-year-old female born to a non-consanguineous Australian/Caucasian couple where the pregnancy was complicated by premature labour and vaginal bleeding at six months gestation, which spontaneously stopped. She was born with a single umbilical artery at term, with a birth weight of 3500 g and head circumference of 34.5 cm, in poor condition, which improved quickly and she was discharged from hospital a few days later. Postaxial polydactyly of both feet and right hand was noted after birth, and these extra digits were surgically removed in later childhood. After a period of poor feeding in infancy, she re-presented to hospital at five weeks with cyanotic heart disease requiring open-heart surgery to repair a complete atrioventricular septal defect with common atrium. She had persistent pneumonia and cardiac failure post-surgery and was discharged at 3 months of age. Developmentally, she smiled at 3-4 months of age, rolled at 13 months of age, laughed at 15 months and walked at five years of age with assistance after developmental regression at two years of age with loss of speech. An early pelvic X-ray showed prominent iliac wings with a notch below the sacroiliac joints (films not available for review). She had refractory focal epilepsy with onset of focal impaired awareness seizures (FIAS) at eight years of age and developed aggressive behaviour at 9 years. She had a single episode of nonconvulsive status epilepticus (NCSE) at ten years of age and also has nocturnal tonic seizures. In adulthood, she has severe intellectual disability with limited mobility, autistic features and mild generalised spasticity. She has a history of multiple several tumors including a grade 1 borderline mucinous ovarian tumour at 17 years, liver haemangioma, and a renal cell carcinoma at 17 years. Other history includes hyperprolactinaemia attributed to haloperidol use for aggression, deformed tympanic membranes with good hearing, atrial fibrillation with persistent valvular incompetence, osteoporosis with multiple fractures resulting in her being unable to weight-bear or walk from 38 years, dural ectasia, recurrent dislocated patellae, and gastroesophageal reflux disease.

On examination in adulthood, she had an asthenic build and normal stature. Facially, she had a broad forehead, hypertelorism, prognathism, and a prominent nasal tip and an asymmetric nasal bridge related to a prior fracture. There was no obvious midline cleft of her lip or tongue, or accessory oral frenula. Her ear morphology and position looked normal. She had broad toes, mild digital clubbing, fifth finger clinodactyly, and scars on her feet and right hand from previous polydactyly surgery.

Her investigations included MR brain that documented asymmetric brachycephaly with a prominent pituitary, and an EEG showed right centro-parietal slowing. Bone densitometry revealed low for age bone mineral density with a lowest T-score of -2.6 in AP spine. Her serum corrected calcium (2.35 mmol/L (2.15-2.65)) and her phosphate (1.2 mmol/L (0.8-1.4)) levels were normal. She also had normal serum 25-hydroxy vitamin D (126 nmol/L (>50)). Her serum prolactin was elevated at 942 mIU/L (59-619) and she has had slightly low thyroid stimulating hormone (TSH; 0.32 mIU/L (0.50-4.00)) with normal free thyroxine (FT4;15.5 pmol/L (10.0-19.0)). She had no adrenal lesions reported on abdominal CT or ultrasound imaging.

Supplemental Figures

Figure S1

Figure S1. Cα and Cβ mutated residues are evolutionarily conserved. Each panel shows a stretch of amino acids from human Cα (*PRKACA*) or Cβ (*PRKACB*) comprising the mutated residues found in affected individuals (red letters) aligned to the corresponding sequences of Cα and Cβ PKA subunits from different vertebrates. The sequences of homologous cAMP-dependent protein kinase catalytic subunits from three invertebrates are also shown. *Homo sapiens* (*Hs*), *Mus musculus* (*Mm*), *Xenopus laevis* (*Xl*), *Danio rerio* (*Dr*), *Drosophila melanogaster* (*Dm*), *Caenorhabditis elegans* (*Ce*), *Aplysia californica* (*Ac*). Residues that are non-identical to the human proteins are in black letters. Protein reference numbers are indicated.

Figure S2. WES Results and Analysis Pipelines

Individual 1

total number of single nucleotide variations (SNVs)	MAF (gnomAD v2.1.1. liftOver hg38) ≤ 0.001	loss-of function variants or missense	CADD PHRED score >20 and polyphen2 predicted damaging	Present in affected daughter (II-3)	Genes in common with WES results from individual 2
143223	12262	719	194	69	1

Individual 2

Total number of SNVs	variants present in affected foetus (III-3)	MAF gnomAD ≤ 0.001	Coding nonsynomymous variants, indels or splicing variants	CADDv1.4 >20 and Polyphen2 predicted damaging	Genes in common with WES results from individual 1
58483	23709	472	118	40	1

Comparison of WES results between families 1 and 2 with very similar phenotypes identified only one gene in common: *PRKACA*. All affected individuals from both families carried the same *PRKACA* variant NM_002730.4: c.409G>A (p.Gly137Arg). Individual 1 was also heterozygous (VAF:0.49) for a misssense variant of uncertain significance in *GPR161*: NM_001267609.1: c.263G>A (p.Ser88Asn) that was among the 69 variants present in his affected daughter (II-3 in Figure 1A). Heterozygous variants in *GPR161* have been associated with risk of spina bifida[1] and in a consanguineous family, a recessive missense variant in *GPR161* was associated with Pituitary Stalk Interruption Syndrome[2]**.**

Individual 4

Total number of SNV	Variants with allele frequency < 1% in ALL population from the phase III of the 1000 Genomes Project	Coding nonsynomymous variants, indels or splicing variants	Variants classed as deleterious at least by half of four pathogenicity predictors (SIFT, Polyphen, Mutation Taster, CADD)	Recessive model	*De novo*
358133	41152	1382	794	92	6

Manual inspection identified the *PRKACB* (NM_002731.3) *de novo* variant c.703G>C (p.Gly235Arg) as the likely cause of the disease. The rest of variants were overrepresented in control population databases (dbSNP) or corresponded to polymorphic indel positions.

Individual 5

Total number of SNV	Variants with allele frequency < 1% in dbSNP, 1000 genomes, Exome Variant Server, Exac, gnomAD	Coding nonsynomymous variants, indels or splicing variants	Variants in neither "In-House" exomes	Variants considered by SIFT or Polyphen as surely damaging and CADD score >30
122765	18718	4950	90	3

Selected variant: *PRKACB*: c.161C>T (p.Ser54Leu). Other WES findings of uncertain significance: *USP40*: c.1586G>A (p.Arg529Lys); *ADAD2*: c.1795C>T (p.Arg599Cys).

Individual 6

Total number of SNVs	MAF gnomAD ≤ 0.01%	Removing intergenic or non-coding variant	CADD≥20 and damaging by Polyphen or SIFT	Inheritance mode and BAM validation
45812	3831	993	130	1

Selected variant: *PRKACB*: c.263A>G (p.His88Arg)

Individual 7

Total number of SNVs	Exonic or splicing	Remove synonymous SNVs	Filter gnomAD allele frequency	Filter inheritance model	Manually inspected
495726	36200	22392	1321	60	3 (one proven to be a sequence artefact by Sanger sequencing validation)

Selected variant: *PRKACB*: c.262C>A (p.His88Asn). Other WES findings of uncertain significance: *PIGR*: c.155G>A (p.Arg52Gln (*de novo*)).

Figure S3

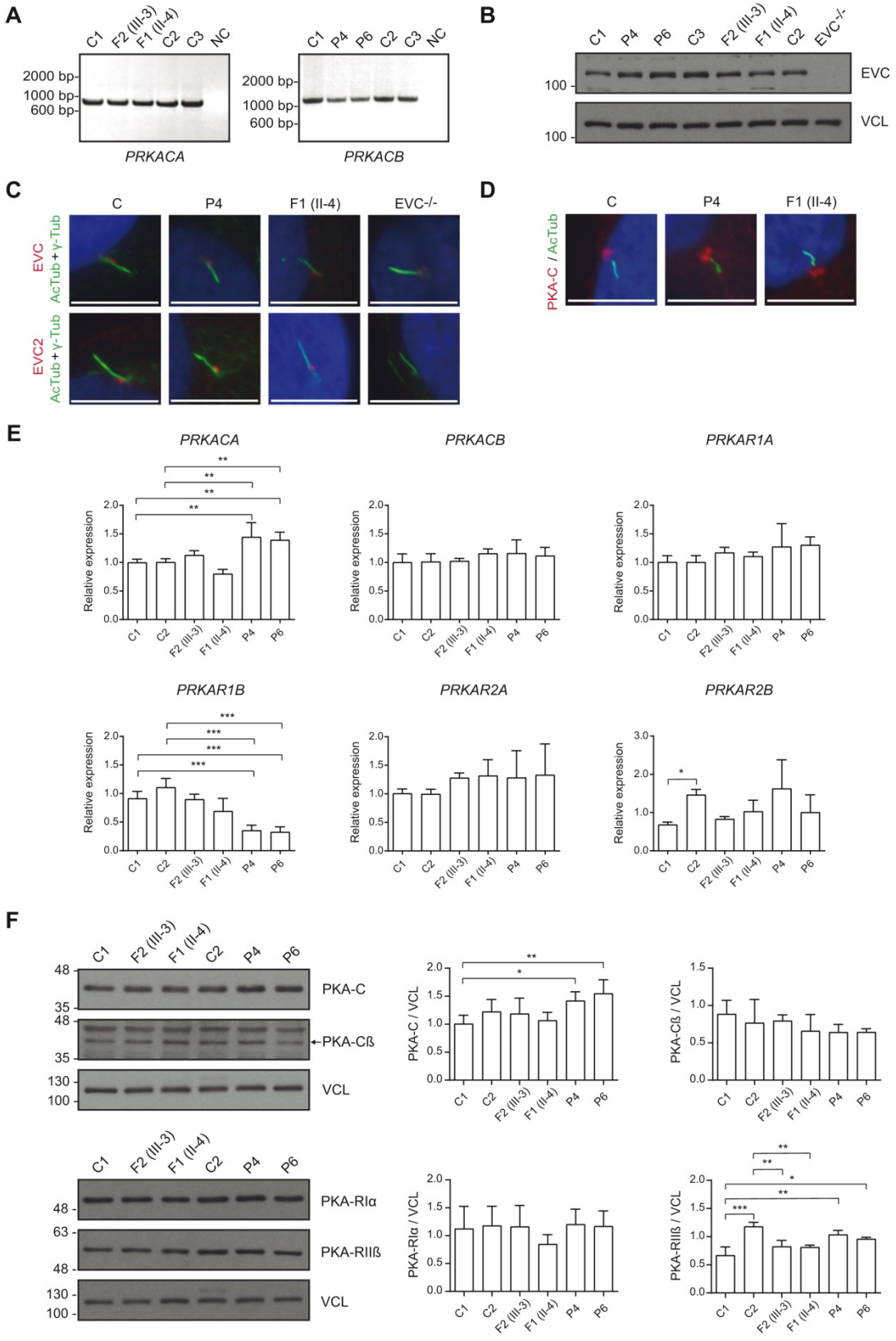
A
C1
F2 (III-3)
F1 (II-4)
C2
C3
NC
2000 bp
1000 bp
600 bp
PRKACA
PRKACB
B
P4
P6
EVC-/-
EVC
VCL
100
C
P4
F1 (II-4)
EVC-/-
EVC
AcTub + γ-Tub
EVC2
D
PKA-C / AcTub
E
PRKACA
PRKACB
PRKAR1A
PRKAR1B
PRKAR2A
PRKAR2B
Relative expression
F
PKA-C
PKA-Cß
PKA-RIα
PKA-RIIß
PKA-C / VCL
PKA-Cß / VCL
PKA-RIα / VCL
PKA-RIIß / VCL

Figure S3. Expression analysis of EvC proteins and of PKA-C and PKA-R transcripts and proteins in primary fibroblasts. **A.)** RT-PCR demonstrating expression of both *PRKACA* and *PRKACB* transcripts in fibroblasts from controls (C1 and C2) and affected individuals (F2(III-3) and F1(II-4): Cα-p.Gly137Arg; P4: Cβ-p.Gly235Arg; P6: Cβ-p.His88Arg [P: proband, F: family; family members are named as in Figure 1A]). NC is a negative control with no template. For each gene a forward primer upstream of the corresponding mutations and a reverse primer placed at the 3'-UTR were used (see methods for primer sequences). Direct sequencing of the amplified cDNA products confirmed the presence of the corresponding heterozygous missense mutations in samples from affected individuals indicating expression of both normal and mutant alleles. **B.)** Western Blot (WB) analysis of primary fibroblasts showing similar protein levels of EVC between normal controls (C) and affected subjects. Vinculin (VCL) was used as loading control. n=2. **C.)** Immunofluorescence images (shifted overlay) showing normal EVC and EVC2 localization at the base of primary cilia in fibroblasts from control (C) and affected individuals (P4 and F1(II-4)). $EVC^{-/-}$ cells carrying loss of function mutations were used as negative control[3], n=2. Red: EVC or EVC2; green: acetylated-tubulin (AcTub) and γ-tubulin (γ-Tub); blue (DAPI): nuclei. Scale bars: 10 μm. **D.)** Immunofluorescence images showing PKA-C localization at the base of primary cilium of fibroblasts derived from control (C) and affected individuals (P4 and F1(II-4)), n=3. Red: PKA-C; green: acetylated-tubulin (AcTub); blue: nuclei. Scale bars: 10 μm. **E.)** Relative mRNA quantification of PKA-C (*PRKACA*, *PRKACB*) and -R subunits (*PRKAR1A*, *PRKAR1B*, *PRKAR2A*, *PRKAR2B*) by qRT-PCR using TaqMan probes in fibroblasts from two independent normal controls (C1 and C2) and affected individuals (F2(III-3), F1(II-4), P4, P6). Values were normalized to *ACTB* and *GUSB* mRNA levels and represented as fold change of the mean value of C1 and C2. Graphs show means ± SD, n = 4. * = P ≤ 0.05, ** = P ≤ 0.01, *** = P ≤ 0.001 by one-way ANOVA followed by Tukey or Dunn's post-hoc test. **F.)** WB analysis of PKA-C, PKA-Cβ, PKA-RIα and PKA-RIIβ in fibroblasts from controls and affected individuals. The PKA-C antibody used (BD Transduction Laboratories (610980)) is raised against the Cα-subunit, but due to amino acid conservation, we observed that it can recognize both Cα and Cβ-subunits in extracts from cells transfected with individual FLAG-tagged C-subunits. Representative immunoblots are on the left and histograms show densitometric quantification of the different proteins referred to vinculin (VCL) that acted as loading control. Data are expressed as mean ± SD, n=4 (PKA-C, PKA-Cβ); n=3 (PKA-RIα, PKA-RIIβ). * = P ≤ 0.05, ** = P ≤ 0.01, *** = P ≤ 0.001 by one-way ANOVA followed by Tukey post-hoc test.

Figure S4

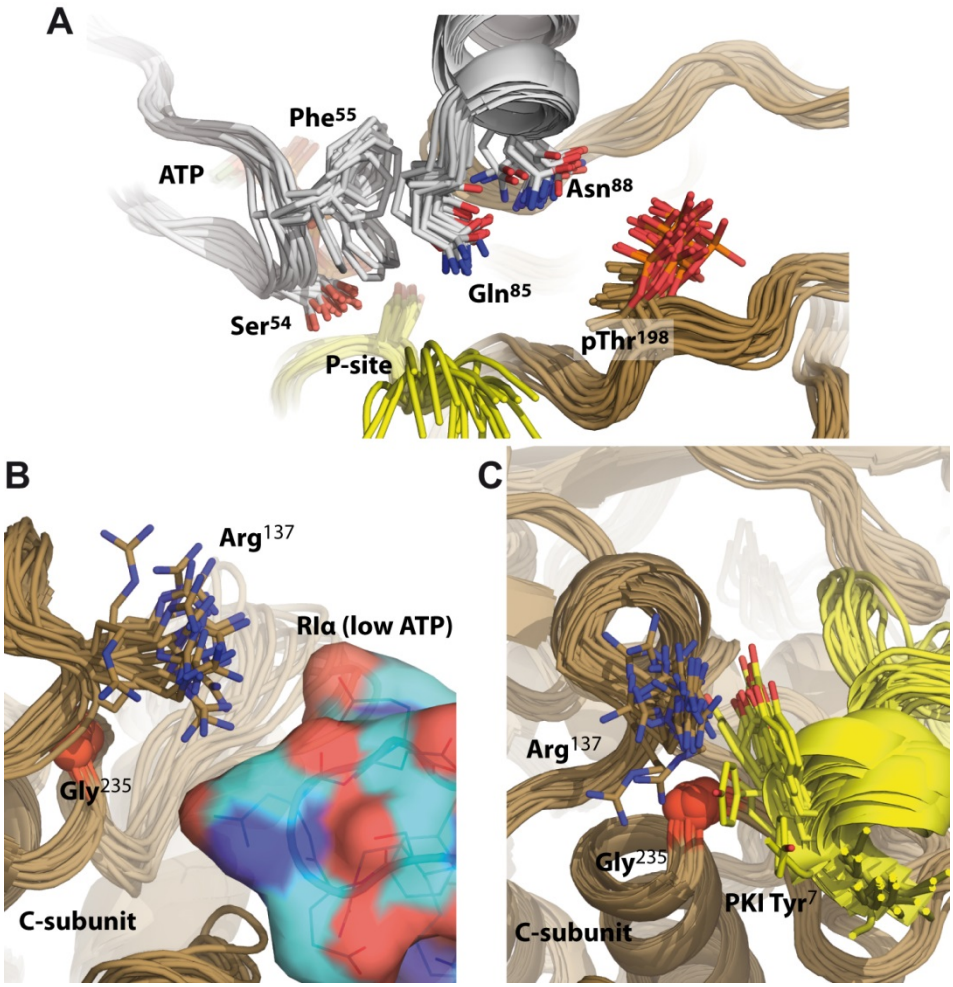

Figure S4. Effect of mutations on dynamics. A.) A change in G-loop dynamics compared to WT is observed in simulations for the Cβ-p.His88Asn mutation. This is similar to the Cβ-p.His88Arg mutation and likely leads to a change in synergistic ATP and substrate peptide binding**. B.)** The cAMP binding domain-B of RIα docks into the pocket of the C-subunit perturbed by p.Gly137Arg and p.Gly235Arg mutants. This interaction is only observed in the low-ATP bound form of the RIα holoenzyme[4]. **C.)** The tethering helix of PKI (5-24) also forms an interface with p.Gly137Arg and p.Gly235Arg.

Figure S5

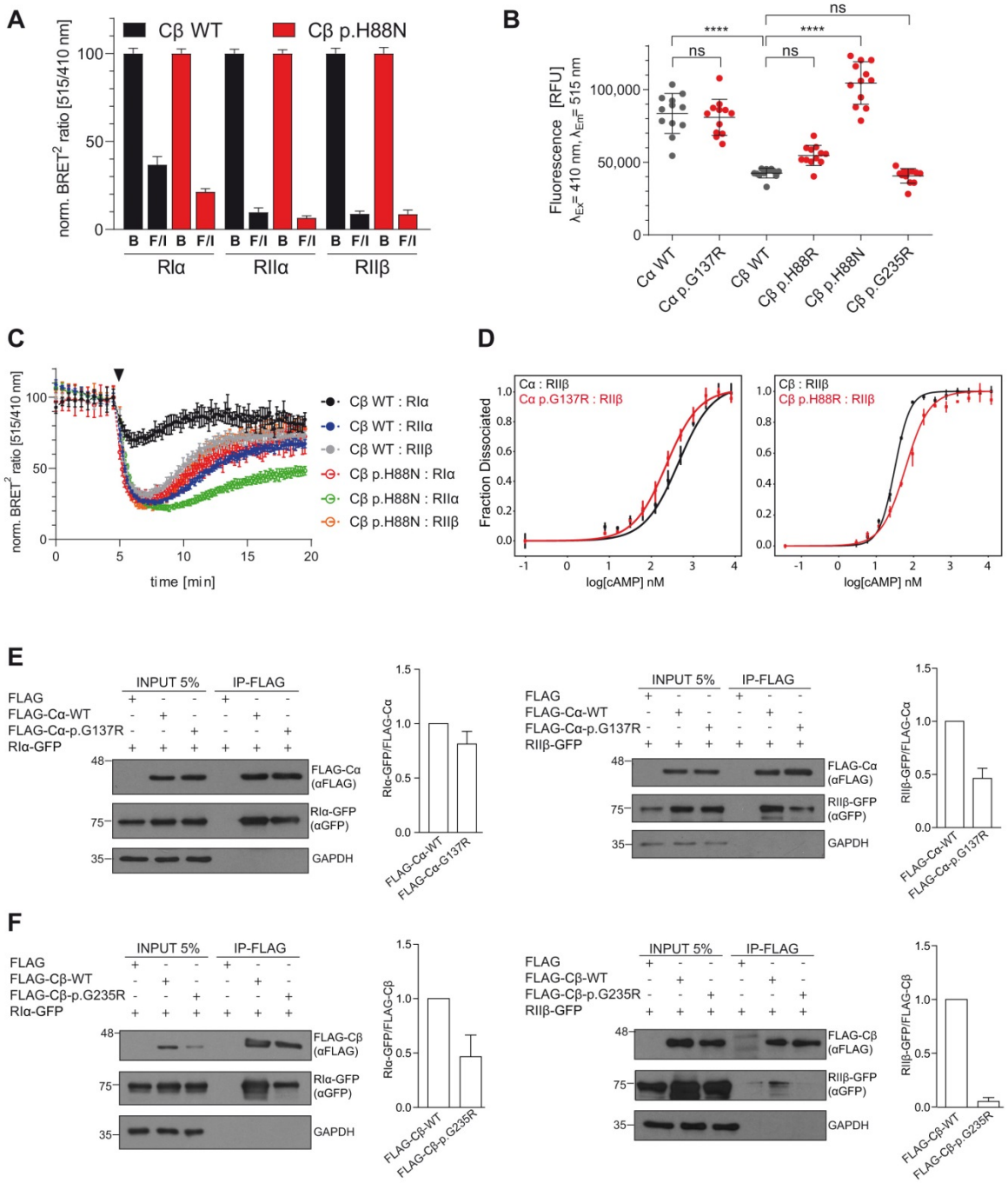

Figure S5. Functional characterization of PKA holoenzymes. A.) BRET^2 for Cβ-p.His88Asn (for conditions see figure legend 2E) demonstrating almost full dissociation upon F/I. Normalized data are shown as means (± SD) of 3 independent experiments with n=6 replicates each (total n=18). **B.)** Expression levels of GFP-tagged PKA-C-subunits in HEK293 cells: Cα-WT has a higher expression level compared to Cβ-WT while the mutant Cβ-p.His88Asn has a higher expression level than Cβ-WT. Statistics were done by one-way ANOVA followed by a Dunnett's Multiple Comparison (**** = P ≤ 0.0001, ns = not significant) using n=12 replicates. **C.)** BRET^2 Kinetics for Cβ-p.His88Asn (for conditions

see Figure 2F) showing a reduced response after 100nM isoproterenol compared to Cβ-p.His88Arg. Data shown are means ± SD of n=6 replicates showing one of 3 (2 for RIIα) independent experiments. **D.)** FPA on RIIβ. The Cα-p.Gly137Arg:RIIβ holoenzyme is easier to activate by cAMP compared to WT. The Cβ-p.His88Arg:RIIβ holoenzyme has an apparent decreased sensitivity to cAMP, however this is likely an artifact of the FPA experiment where the signal is dependent on fluorescent-PKI(5-24) peptide competing off the inhibitor segment of the holoenzyme regulatory subunit – the 10 fold decrease in PKI peptide affinity for Cβ-p.His88Arg increases the apparent activation constant (n=3). Graphs show mean ± SD. **E-F.)** Co-immunoprecipitation (Co-IP) analysis. FLAG-immunoprecipitation from HEK293T co-transfected with the indicated constructs showing decreased interaction of Cα-p.Gly137Arg and Cβ-p.Gly235Arg with regulatory subunits RIα or RIIβ with respect to the corresponding WT proteins. Plasmids included in each transfection are marked as +. GAPDH levels acted as loading control. Bar graphs show RIα-GFP/FLAG-Cα or RIIβ-GFP/FLAG-Cα ratio calculated by densitometry from the blots on the left. In each blot values were normalized to the value of the WT protein, n=3. Data are mean ± SD.

Figure S6

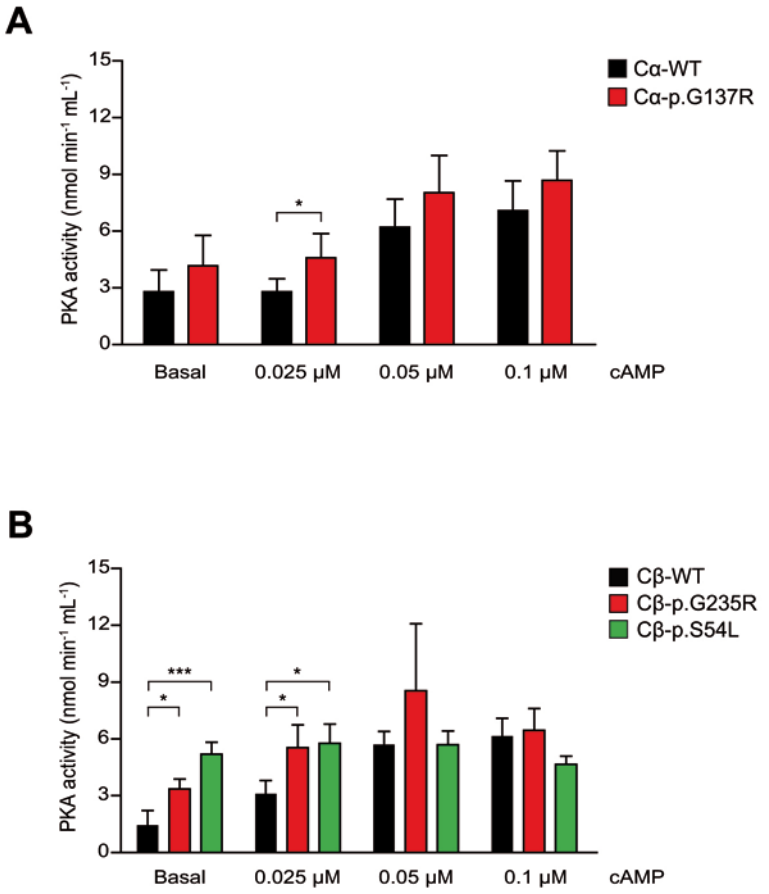

Figure S6. Effect of *PRKACA* and *PRKACB* mutations on PKA kinase activity. **A-B.)** PepTag assay using extracts from HEK293T co-transfected with FLAG-C and RIα-GFP subunits. This experiment revealed higher kinase activity of Cα-p.Gly137Arg compared to Cα-WT at 0.025 µM of cAMP (A). Cβ-p.Gly235Arg also shows higher kinase activity than Cβ-WT both at basal and after addition of 0.025 µM of cAMP. This is comparable with the previously reported activating PKA mutation, Cβ-p.Ser54Leu, which was included as control[5] (B). Data represent the mean ± SD of four independent experiments. * = P ≤ 0.05; *** = P ≤ 0.001 by one-way ANOVA followed by Tukey post-hoc test.

Figure S7

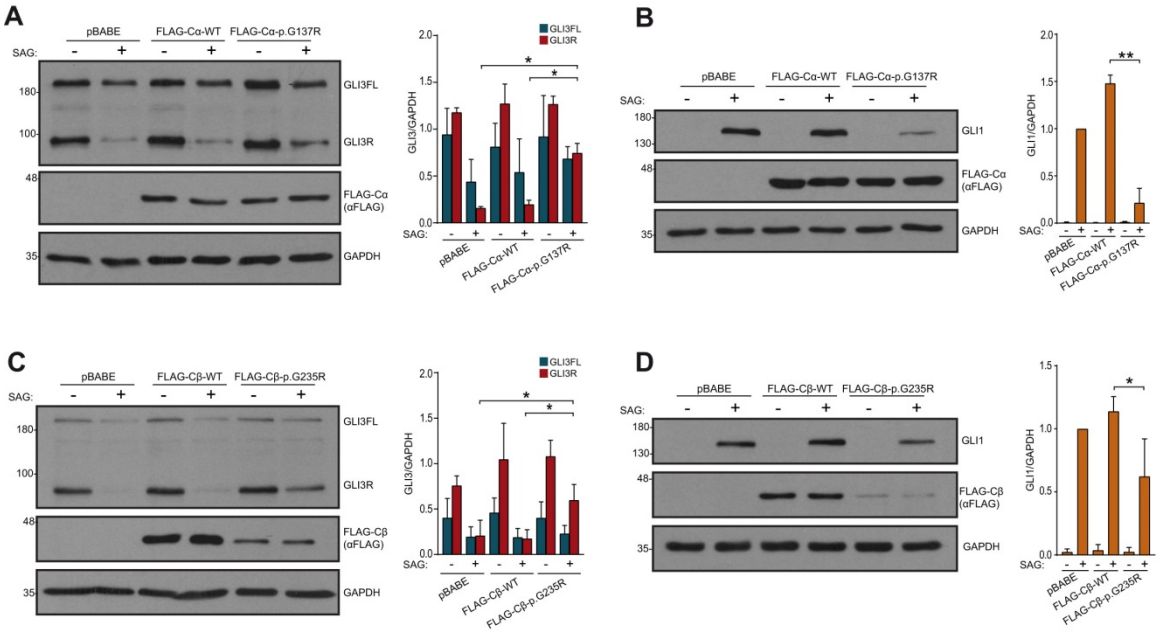

Figure S7. Impact of *PRKACA* and *PRKACB* mutations in Hh signaling evaluated in NIH 3T3 retrotransduced only with C-subunits. **A-D.)** Analysis of GLI3 and GLI1 protein levels in NIH 3T3 retrotransduced with human FLAG-Cα-WT or FLAG-Cα-p.Gly137Arg retroviral vectors (A-B), or alternatively, with FLAG-Cβ-WT or FLAG-Cβ-p.Gly235Arg retroviruses (C-D), exposed to SAG (+) or its vehicle DMSO (-). Expression levels of FLAG-C are shown in the underneath panels. After incubation with SAG, Cα-p.Gly137Arg and Cβ-p.Gly235Arg retrotransduced cells showed increased levels of GLI3R and reduced amount of GLI1 in comparison to cells retrotransduced with pBABE (empty vector) or with FLAG-Cα-WT or FLAG-Cβ-WT. Representative immunoblots are on the left and histograms represent densitometric quantification of the levels of GLI3R and GLI3FL referred to GAPDH (A and C) or GLI1/GAPDH levels normalized to the value of SAG-pBABE cells (B and D). Data are expressed as mean ± SD from two, (A-B) or three (C-D) independent retroviral infections. * = $P < 0.05$; ** = $P < 0.01$; Student's t-test.

Figure S8

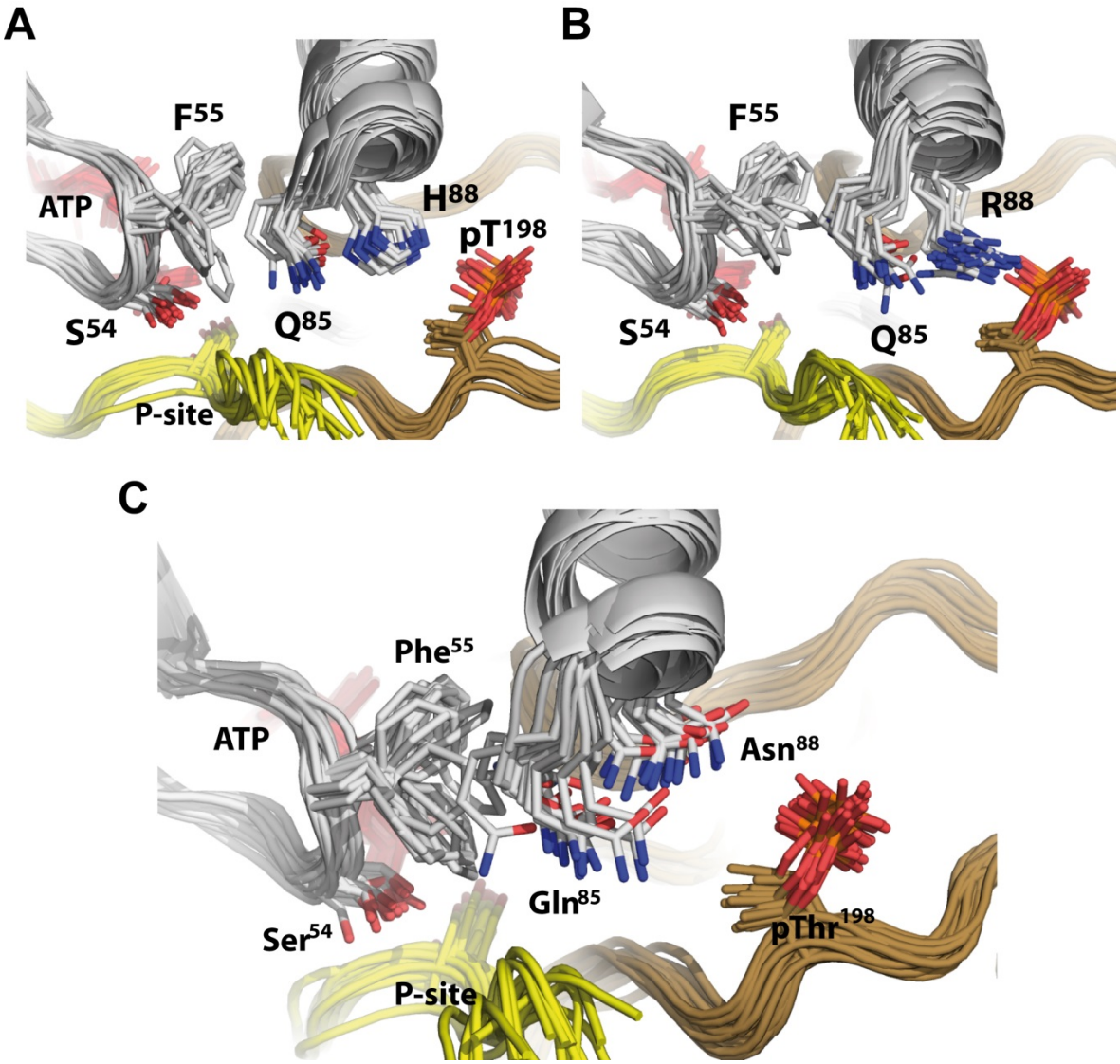

Figure S8. Molecular dynamics (MD) simulations of non-canonical Cβ1 isoform sequence (BC035058). Images illustrate identical effects on dynamics due to disease mutation as MD simulations of canonical Cβ1 sequence NM_002731 shown in Figure 2A-B and S4A. Panels A, B and C correspond to Cβ-WT, -p.His88Arg and -p.His88Asn, respectively.

Supplemental Tables

Table S1. Binding and activation constants for Cβ-p.His88Arg and Cα-p.Gly137Arg

		Cα-WT	Cα-p.Gly137Arg	Cβ-WT	Cβ-p.His88Arg
C:ligand					
IP20	Kd	1.12 ± 0.05 nM*	0.73 ± 0.04 nM*	3.7 ± 0.1 nM	37.1 ± 1.8 nM
ATP	EC_{50}	94.0 ± 3.5 nM	54.4 ± 2.5 nM	182.0 ± 11.8 nM	6000 ± 7000 nM
C2:R2 cAMP activation					
RIα : C	EC_{50}	8.15 ± 0.22 nM	4.41 ± 0.15 nM	24.2 ± 1.4 nM	15.1 ± 1.8 nM
	Hill	1.39 ± 0.05	1.36 ± 0.05	1.01 ± 0.05	1.04 ± 0.11
RIIβ : C	EC_{50}	440.8 ± 47.5 nM	226.9 ± 16.6 nM	31.3 ± 1.0 nM	60.1 ± 3.4 nM†
	Hill	1.07 ± 0.11	1.11 ± 0.08	2.11 ± 0.12	1.36 ± 0.09

Kd: dissociation constant. EC50: apparent half maximal effective concentration. Hill: Hill coefficient.
*1nM detectable limit, † EC50 is dominated by FAM-IP20 low affinity binding. Fitted values show the standard error of the mean (SEM).

Supplemental Methods

Genetic analysis

Peripheral blood genomic DNA was used in all genetic studies. Mutations in EvC-responsible genes *EVC* and *EVC2* were excluded in four individuals (P1-P4) by direct Sanger sequencing of all coding exons of both genes and MLPA analysis (MRC-Holland) (P1, P2, P4), or by means of a gene-targeted NGS clinical panel (P3). Trio (proband and both parents)-whole exome sequencing (WES) was performed in families 2, 4, 6 and 7 using standard DNA capture and variant filtering methodology. In family 5 only the affected child was analyzed by WES. In family 1, WES was conducted in the proband, one affected daughter (II-3 in Figure 1A) and her mother. WES was also performed in the affected fetus of family 2. In P3, *PRKACA* and *PRKACB* were screened by Sanger sequencing. In addition to standard WES, high-depth WES was carried out in P1 and the father of P2 to further confirm the mosaic state of the detected mutation.

Ensemble modeling by Molecular Dynamics

All complexes were prepared from the crystal structure of PKA in a closed ternary conformation bound with PKI (5-24) inhibitor peptide, ATP, and two Mn+2 ions (PDB code 3FJQ)[6]. The sequence was modified to match human PRKACA (NM_002730) or PRKACB (β1 isoform BC035058 and NM_002731), Mn ions were changed to Mg, and Ser140, Thr198 and Ser339 were phosphorylated. N-terminal residues that were missing due to disorder in the original crystal structure were built based on the N-terminal structure of myristylated PKA (PDB code 1CMK)[7], removing the myristyl moiety from the models. Mutations for Cβ-p.His88Arg/Asn and Cα-p.Gly137Arg were generated from the wild-type models. The inhibitor peptide was mutated to the pseudo-substrate sequence PKS: TTYADFIASGRTGRRASIHD. The RIIβ inhibitory segment was taken from the RIIβ crystal structure (PDB code 3TNP)[8], AGAFNAPVINRFTRRASVCAEAYNPD, and superposed onto the human PKA models. Five complexes, Cβ-p.His88Arg:PKS, Cβ-p.His88Asn:PKS, Cβ:PKS, Cα-p.Gly137Arg:RIIβ, and Cα:RIIβ were generated. Hydrogens and counter ions were added and the models were solvated in a cubic box of TIP4P-EW water[9] and 150mM KCl with a 15 Å buffer in AMBERtools[10]. Parameters from the Bryce AMBER Parameter Database were used for ATP[11], phosphothreonine[12], and phosphoserine[12]. Protonation states of histidines were optimized for neutral pH, specifically H88 was protonated. AMBER16[10] was used for energy minimization, heating, and equilibration steps, using the GPU DPFP code for minimization and the GPU SPFP code for heating and equilibration.

Systems were minimized by 1000 steps of hydrogen-only minimization, 2000 steps of solvent minimization, 2000 steps of ligand minimization, 2000 steps of side-chain minimization, and 5000 steps of all-atom minimization. Systems were heated from 0 K to 300 K linearly over 250 ps with 2 fs time-steps and 5.0 kcal·mol·Å position restraints on backbone atoms. Temperature was maintained by the Langevin thermostat. Constant pressure equilibration with a 10 Å non-bonded cut-off was performed with 300 ps of backbone restraints followed by 510 ps without restraints. A 10 Å cut-off for non-bonded interactions with particle mesh Ewald was used for a final 4 ns of equilibration. Production simulations were performed on GPU enabled AMBER16 for 1 ns. 20 independent minimization, equilibration, and production runs of each of the four complexes were performed. All atom RMSD was used to confirm equilibration of the system. The last frame of each trajectory was used as a representative model in the ensemble. The RIα (PDB code 6NO7)[4] holoenzyme structure was superposed with the models to illustrate the effect of mutations on the holoenzyme complex.

Bioluminescence resonance energy transfer ($BRET^2$) assays

HEK293 cells were seeded in a 96-well microplate (Nunclon™ Delta Surface; Thermo Scientific) with a density of 2 x 10^4 cells per well cultured in DMEM (Capricorn Scientific) supplemented with 10 % FCS (Capricorn Scientific). Cells were transiently cotransfected with GFP^2-tagged PKA Cα-WT/Cβ1-WT or a mutant (Cα-p.Gly137Arg, Cβ1-p.His88Arg, Cβ1-p.His88Asn, Cβ1-p.Gly235Arg) and the respective Rluc8-tagged[13] PKA regulatory subunit at a total of 0.05 µg DNA per construct using polyethyleneimine (25 kDa, Polysciences GmbH) as previously described[14]. The reporter proteins were expressed for 46-48 h at 37°C and 6 % CO_2. For endpoint measurements, cells were washed with Hanks' balanced salt solution (HBSS; Biowest) and incubated with 50 µM Forskolin (Sigma-Aldrich) and 100 µM IBMX (Sigma-Aldrich) or HBSS alone (untreated control) for 20 minutes prior to adding 5 µM Coelenterazine 400A, a luciferase substrate (DeepBlueC™; BIOTREND Chem)[15]. Emitted light was detected using a POLARstar Omega microplate reader (dual emission optics; BMG Labtech) with filters at wavelengths 410 ± 80 nm (Rluc8, donor) and 515 ± 30 nm (GFP^2, acceptor). Cells expressing Rluc8 alone were used as control for each experiment. By using GraphPad Prism 8.0 (GraphPad Software), the mean values (± standard deviation) were calculated from three independent measurements (each from 6 replicates), if not indicated otherwise. Data were normalized between the signal of unstimulated cells (buffer (B) only = 100%) and the Rluc8 control signal (0%). For kinetic measurements, transfected cells were washed with HBSS before the reaction was started upon the addition of 5 µM Coelenterazine 400A

with a total measuring time of 20 minutes. Different concentrations of isoproterenol (Sigma-Aldrich) were injected after 5 minutes at a final concentration of 100 nM in HBSS supplemented with 5 µM Coelenterazine 400A. For application into the wells the reagent injector of the microplate reader was used. $BRET^2$ ratios were calculated from the 515 nm (GFP^2-signal) to 410 nm (luciferase-signal) ratio. Data was analyzed with GraphPad Prism 8.0 by plotting the normalized $BRET^2$-ratio against the time (kinetic measurements).

For quantification of expression level, cells were transiently transfected with the respective GFP^2-tagged C-subunit (Cα-WT, Cα-p.Gly137Arg, Cβ1-WT, Cβ1-p.His88Arg, Cβ1-p.His88Asn, Cβ1-p.Gly235Arg) and treated as described for untreated controls in the endpoint $BRET^2$ measurements. Data point acquisition took place with a CLARIOstar microplate reader (BMG Labtech) at excitation and emission wavelength of 410 ± 8 nm and 515 ± 10 nm, respectively. Each well was scanned in a 10x10 scan matrix (5 mm diameter) with 8 flashes per scan point. Gain adjustment of fluorescence was set at 10% of the maximum fluorescence intensity (260,000 RFU, relative fluorescence units) against the Rluc8 control well (cells only transfected with Rluc8 without GFP^2-tagged protein transfection). Data were analyzed with GraphPad Prism 8.0 by plotting obtained fluorescence intensity as scatter dot blot with mean ± SD against the transfected constructs. For $BRET^2$ and the rest of experimental procedures NM_002730.4 (Cα) and NM_002731.3 (Cβ1) reference sequences were used unless otherwise specified.

Co-immunoprecipitation (Co-IP)

Mutant Cα and Cβ1 subunits were generated by directed mutagenesis using QuikChange II Site-Directed Mutagenesis Kit (Agilent Technologies) or amplified from fibroblast cDNA of affected individuals generated with superscript IV (Life Technologies). C- and R-subunits were cloned into pFLAG-CMV4 and pEGFP-N1, respectively. For transfections, HEK293T were cultured in growth medium (Dulbecco's modified Eagle's medium (DMEM) supplemented with 10% fetal bovine serum (FBS) and 1 X antibiotic-antimycotic (Gibco)) at 37°C and 5% (v/v) CO_2. Cells were seeded at a density of $2.5x10^6$ cells/P100 and co-transfected by the calcium phosphate method with a DNA mix containing 5 µg of a FLAG-Cβ1 plasmid and 5 µg of a construct carrying RIα-GFP or RIIβ-GFP. In co-transfections using FLAG-Cα subunits, 2 µg of C- and 2 µg of R-constructs were used. Cells were lysed 44 h after transfection in immunoprecipitation buffer 1X (Dynabeads Co-Immunoprecipitation Kit, Life technologies, 14321D) containing protease inhibitors and 150mM (RIα Co-IP) or 300mM (RIIβ Co-IP) of NaCl. Subsequently, 500 µg (Cβ Co-IP) or 200 µg (Cα Co-IP) of protein extracts were incubated with 10 µg of anti-FLAG M2

Magnetic beads (M8823, Sigma-Aldrich) and maintained 1 h in rotation at RT. Following three washes with TBS 1X, the beads were boiled in Laemmli sample buffer containing DTT (100 mM) for 5 min and processed for Western Blotting.

Western blot

Western blot (WB) analysis was performed as previously described[3]. Cell lysis was carried out in RIPA buffer (50 mM Tris–HCl pH 7.5, 150 mM NaCl, 2 mM EDTA, 1% NP40, 0.1% SDS, 0.5% Sodium deoxycholate) supplemented with protease and phosphatase inhibitors (Sigma, P8340, P0044 and P5726, 2.5 mM Na_3O_4V and 10 mM NaF). Primary antibodies: anti-mouse GLI1 (1:500; Cell Signaling, L42B10), anti-human/mouse GLI3 (0.4 µg/mL; R&D, AF3690), anti-α-Tubulin (1:80000; Sigma, T9026), anti-human EVC (1:1500; Sigma, HPA016046), anti-PKA-C (1:1000; BD Transduction Laboratories, 610980), anti-Cβ (1:1000, antisera SNO157)[16], anti-RIα (1:1000,Cell Signaling, 5675), anti-RIIβ (1:1000, BD Transduction Laboratories, 610625), anti-Vinculin (1:2000; Santa Cruz sc-73614), anti-GAPDH (1:10000; Thermo Fisher, AM4300), anti-FLAG (1:2000 in Co-IPs, 1:500-retroviral infections; Sigma, F1804), anti-GFP (1:2000 in Co-IPs, 1:500-retroviral infections; Invitrogen, A6455). HRP-conjugated secondary antibodies were from Jackson ImmunoResearch. Blots were developed with ECL HRP substrate (Amersham) and exposed to X-Ray films. For protein quantification, films were scanned and densitometric analysis was conducted using ImageJ. GraphPad software 8.0 was used for statistical analysis.

Expression and Purification of Recombinant Proteins

The PKA catalytic subunit was expressed in *E. Coli* and purified as previously described[4]. Briefly, human isoforms of PKA-C were inserted into a pET15b expression system behind an N-terminal His-6-SUMO tag. The PRKACB (BC035058) sequence contained 3 amino acid differences compared to NM_002731: L163I, H159N, and H261N. These sequence differences likely have little impact on the interpretation since analysis is comparative to WT and the sequence difference is common within WT and disease mutant p.His88Arg. In addition, MD simulations of both canonical (Figure 2A-B and S4A) and non-canonical (Figure S8) Cβ sequences demonstrated identical effects on dynamics due to disease mutation. The PRKACA p.Gly137Arg and PRKACB p.His88Arg mutations were introduced into their respective WT isoform vectors using Phusion Site-Directed Mutagenesis PCR. After bacterial expression and Ni-Sepharose purification the His-SUMO tag was cleaved using His6-Ulp1 while dialyzing overnight at 277.15 K, producing native PKA-C. SUMO,

Ulp1, and uncleaved protein was removed by rebinding to Ni-Sepharose resin. A size exclusion Superdex-75 gel filtration column was used as a final purification step. Type Iα and type IIβ R-subunits were recombinantly expressed and purified as previously described[4]. PKA tetrameric holoenzymes were pre-formed via incubation with R-subunit and C-subunit at a 1:1.3 (R:C) molar ratio and purified over a Superdex-200 gel filtration column to remove excess C-subunit. Type Iα holoenzyme, at ~1 μM, was formed and purified in the presence of 5 mM MgCl2 and 200 μM ATP.

LiReC Fluorescence Polarization Assay (FPA)

The LiReC assay was performed as described previously[17]. In brief, activation experiments were performed using two-fold serial dilutions in assay buffer: 20 mM HEPES pH 7.0, 75 mM KCl, 0.005% Triton-X100, 10 mM MgCl2. Either 12 or 14 concentrations were tested in triplicate. Fluorescence polarization signal was measured 15 min after addition of titrant via GENios Plate-reader (Tecan). The stability of holoenzyme was characterized by titration of 1.95 nM - 8 μM cAMP into 12nM of R:C holoenzyme complex, 2-3 nM FAM-IP20, 1 mM ATP (RIα) or 1 mM AMP-PNP (RIIβ). ATP concentration-dependent binding of IP20 was measured via titration of ATP (14.5 nM to 15 μM) into 2 nM FAM-IP20 and 5 nM of purified C-subunit. The binding affinity of the inhibitor peptide to C-subunit was assessed in the presence of saturating ATP via titration of C-subunit (0.39 nM to 400 nM) in 2nM FAM-IP20 and 1 mM ATP.

PKA activity assay

HEK293T were seeded at density of 3 x 10^6 cells/P100 in growth medium and allowed to grow for 24 h before being transfected with the calcium phosphate method. DNA ratios of 1:8 FLAG-Cα:RIα-GFP and 1:1 FLAG-Cβ1:RIα-GFP were used to facilitate association between C- and R-subunits as previously reported[18]. Twenty-four h after transfection cells were trypsinized, washed in cold PBS, and resuspended in 300 μL of buffer containing 5 mM Tris-HCl (pH 7.4), 2 mM EDTA. Cells were homogenized using an Ultraturrax homogenizer for 20 s on ice and centrifuged at 16000 g for 30 min at 4°C. To measure PKA catalytic activity in cell homogenates the PepTag nonradioactive cAMP-dependent protein kinase assay (Promega) that uses a fluorescent Kemptide as substrate was used following the manufacturer's instructions. Samples were tested in the absence or presence of increasing concentrations of cAMP (0.025 μM, 0.05 μM and 0.1 μM) and the PKA kinase activity was quantified by spectrophotometry after separation of the phosphorylated peptide in an agarose gel. PKA kinase activity was calculated as indicated

in the protocol provided by the manufacturer and is expressed in nanomoles of phosphate transferred to PepTag peptide per min^{-1} mL^{-1} in the reaction. GraphPad software 8.0 was used for statistical analysis.

Retroviral infection

HEK293T cells seeded in P100 plates ($3x10^6$/P100) were co-transfected using the calcium phosphate method with 10 µg of the packaging plasmid pCL-Eco and 10 µg of the pBABE retroviral vector either empty, or carrying the human sequence of a specific N-terminal FLAG-tagged C-subunit, or a RIα-GFP fusion protein. Supernatants were collected 44, 52 and 70 h post-transfection and filtered through a 0.45 µm syringe filter (Millipore). Supernatants were diluted 0.5:0.5:1 of pBABE-FLAG-C: pBABE-RIα-GFP: growth medium with polybrene, and then applied to NIH 3T3 cells seeded at $3x10^5$/P60. In total, three consecutive infections were performed, one after each supernatant collection using polybrene at 8 µg/mL, 4 µg/mL and 8 µg/mL, respectively. Cells were left to recover for 24 h after the last infection, and subsequently were subjected to puromycin (2 µg/mL) selection for 72 h. In experiments in which RIα was not included, NIH 3T3 were infected as indicated above with a ratio 1:1 of supernatant containing FLAG-tagged-C-subunit retroviruses and growth medium. Puromycin resistant NIH 3T3 cells were plated at a density of $1×10^6$ cells/P100 in growth medium and 24 h later transferred to low serum medium (DMEM with 0.5% FBS and 1 X antibiotic-antimycotic (Gibco)) supplemented with SAG (100nM, Calbiochem) or its vehicle DMSO (Sigma-Aldrich) and maintained for another 24 h before being analyzed by WB.

RT-PCR and qRT-PCR

Total RNA was purified from primary fibroblasts with TriReagent solution (Sigma-Aldrich) according to manufacturer's instructions and used to synthesize cDNA with SuperScript™ IV First-Strand Synthesis System kit (Invitrogen) and random primers. Fibroblast cDNA was subsequently used as template to amplify a cDNA fragment of *PRKACA* and other of *PRKACB* with GoTaq DNA polymerase (Promega). Forward primers were located upstream of the identified *PRKACA* and *PRKACB* mutations and the reverse primers were from the 3'-UTR of each gene (*PRKACA*-FW: 5'-ATGCCATGAAGATCCTCGAC-3'; *PRKACA*-RV: 5'-ACAGGCATGCCCCTAAAACT-3'; *PRKACB*-FW: 5'-AGGTGGAGAGCGTGAAAGAG-3'; *PRKACB*-RV: 5'-GCTTCAACAAGGACGGTCTC-3'). Amplified products were directly sequenced to confirm the presence of mutant alleles in the heterozygous state in mRNA from affected individuals. For qRT-PCR analysis, total

RNA from fibroblasts was isolated with TriReagent solution and retrotranscribed using the High Capacity cDNA Reverse Transcription Kit (Applied Biosystems). qRT-PCR experiments were performed in a 7900HT Fast Real-Time PCR System (Applied Biosystems) using TaqMan real-time PCR gene expression assays (Applied Biosystems/ Thermo Fisher Scientific). For each line of fibroblasts, RNA from four independent extractions was used and every sample was run in triplicates. Transcript levels were normalized against the geometric mean of two housekeeping genes (*ACTB* and *GUSB*). Fold differences in gene expression were calculated by the $2^{-\Delta\Delta Ct}$ method using the mean of the two normal control cultures included in the analysis as the calibrator sample. Taqman assays were as follows: *ACTB* (Hs99999903_m1), *GUSB* (Hs99999908_m1), *PRKACA* (Hs00427274_m1), *PRKACB* (Hs01086757_m1), *PRKAR1A* (Hs00267597_m1), *PRKAR1B* (Hs00406762_m1), *PRKAR2A* (Hs00177760_m1), *PRKAR2B* (Hs00176966_m1).

Immunofluorescence

Primary fibroblasts were plated onto cover slips in 24-multiwell plates ($1x10^5$/well) in growth medium. After 24 h, the media was replaced to low serum medium for another 24 h. Cells were fixed, permeabilized and incubated with primary and secondary antibodies as previously described[19]. Primary antibodies: acetylated tubulin (Sigma (T7451), 1:2000), γ-tubulin (Sigma (T5326), 1:2000), EVC (Sigma (HPA016046), 1:350), EVC2 (Abcam (ab198930) 1:500) and PKA-C (BD Transduction Laboratories (610980) 1:500). Secondary antibodies (1:1000), DAPI (1:2000) and Prolong Diamond antifade mounting medium were from Molecular Probes.

Supplemental References

1. Kim, S.E., Lei, Y., Hwang, S.H., Wlodarczyk, B.J., Mukhopadhyay, S., Shaw, G.M., Ross, M.E., and Finnell, R.H. (2019). Dominant negative GPR161 rare variants are risk factors of human spina bifida. Hum Mol Genet 28, 200-208.

2. Karaca, E., Buyukkaya, R., Pehlivan, D., Charng, W.L., Yaykasli, K.O., Bayram, Y., Gambin, T., Withers, M., Atik, M.M., Arslanoglu, I., et al. (2015). Whole-exome sequencing identifies homozygous GPR161 mutation in a family with pituitary stalk interruption syndrome. J Clin Endocrinol Metab 100, E140-147.

3. Caparros-Martin, J.A., Valencia, M., Reytor, E., Pacheco, M., Fernandez, M., Perez-Aytes, A., Gean, E., Lapunzina, P., Peters, H., Goodship, J.A., et al. (2013). The ciliary Evc/Evc2 complex interacts with Smo and controls Hedgehog pathway activity in chondrocytes by regulating Sufu/Gli3 dissociation and Gli3 trafficking in primary cilia. Hum Mol Genet 22, 124-139.

4. Lu, T.W., Wu, J., Aoto, P.C., Weng, J.H., Ahuja, L.G., Sun, N., Cheng, C.Y., Zhang, P., and Taylor, S.S. (2019). Two PKA RIα holoenzyme states define ATP as an isoform-specific orthosteric inhibitor that competes with the allosteric activator, cAMP. Proc Natl Acad Sci U S A 116, 16347-16356.

5. Espiard, S., Knape, M.J., Bathon, K., Assie, G., Rizk-Rabin, M., Faillot, S., Luscap-Rondof, W., Abid, D., Guignat, L., Calebiro, D., et al. (2018). Activating PRKACB somatic mutation in cortisol-producing adenomas. JCI Insight 3, e98296. https://doi.org/10.1172/jci.insight.98296.

6. Thompson, E.E., Kornev, A.P., Kannan, N., Kim, C., Ten Eyck, L.F., and Taylor, S.S. (2009). Comparative surface geometry of the protein kinase family. Protein Sci 18, 2016-2026.

7. Zheng, J., Knighton, D.R., Xuong, N.H., Taylor, S.S., Sowadski, J.M., and Ten Eyck, L.F. (1993). Crystal structures of the myristylated catalytic subunit of cAMP-dependent protein kinase reveal open and closed conformations. Protein Sci 2, 1559-1573.

8. Zhang, P., Smith-Nguyen, E.V., Keshwani, M.M., Deal, M.S., Kornev, A.P., and Taylor, S.S. (2012). Structure and allostery of the PKA RIIbeta tetrameric holoenzyme. Science 335, 712-716.

9. Horn, H.W., Swope, W.C., Pitera, J.W., Madura, J.D., Dick, T.J., Hura, G.L., and Head-Gordon, T. (2004). Development of an improved four-site water model for biomolecular simulations: TIP4P-Ew. J Chem Phys 120, 9665-9678.

10. Case DA, B.R., Botello-Smith W, Cerutti DS, Cheatham TE,Darden TA, Duke RE, Giese TJ, Gohlke H, Goetz AW, Homeyer N,Izadi S, Janowski P, Kaus J, Kovalenko A, Lee TS, LeGrand S, Li P,Lin C, Luchko T, Luo R, Madej B, Mermelstein D, Merz KM,Monard G, Nguyen H, Nguyen HT, Omelyan I, Onufriev A, RoeDR, Roitberg A, Sagui C, Simmerling CL, Swails J, Walker RC,Wang J, Wolf RM, Wu X, Xiao L, York DM, Kollman PA. (2016). Amber (University of California, San Francisco).

11. Meagher, K.L., Redman, L.T., and Carlson, H.A. (2003). Development of polyphosphate parameters for use with the AMBER force field. J Comput Chem 24, 1016-1025.

12. Homeyer, N., Horn, A.H., Lanig, H., and Sticht, H. (2006). AMBER force-field parameters for phosphorylated amino acids in different protonation states: phosphoserine, phosphothreonine, phosphotyrosine, and phosphohistidine. J Mol Model 12, 281-289.

13. Loening, A.M., Fenn, T.D., Wu, A.M., and Gambhir, S.S. (2006). Consensus guided mutagenesis of Renilla luciferase yields enhanced stability and light output. Protein Eng Des Sel 19, 391-400.

14. Chepurny, O.G., Bertinetti, D., Diskar, M., Leech, C.A., Afshari, P., Tsalkova, T., Cheng, X., Schwede, F., Genieser, H.G., Herberg, F.W., et al. (2013). Stimulation of proglucagon gene expression by human GPR119 in enteroendocrine L-cell line GLUTag. Mol Endocrinol 27, 1267-1282.

15. Prinz, A., Diskar, M., and Herberg, F.W. (2006). Application of bioluminescence resonance energy transfer (BRET) for biomolecular interaction studies. Chembiochem 7, 1007-1012.

16. Orstavik, S., Funderud, A., Hafte, T.T., Eikvar, S., Jahnsen, T., and Skalhegg, B.S. (2005). Identification and characterization of novel PKA holoenzymes in human T lymphocytes. FEBS J 272, 1559-1567.

17. Saldanha, S.A., Kaler, G., Cottam, H.B., Abagyan, R., and Taylor, S.S. (2006). Assay principle for modulators of protein-protein interactions and its application to non-ATP-competitive ligands targeting protein kinase A. Anal Chem 78, 8265-8272.

18. Bathon, K., Weigand, I., Vanselow, J.T., Ronchi, C.L., Sbiera, S., Schlosser, A., Fassnacht, M., and Calebiro, D. (2019). Alterations in Protein Kinase A Substrate Specificity as a Potential Cause of Cushing Syndrome. Endocrinology 160, 447-459.

19. Palencia-Campos, A., Ullah, A., Nevado, J., Yildirim, R., Unal, E., Ciorraga, M., Barruz, P., Chico, L., Piceci-Sparascio, F., Guida, V., et al. (2017). GLI1 inactivation is

associated with developmental phenotypes overlapping with Ellis-van Creveld syndrome. Hum Mol Genet 26, 4556-4571.